

ATOMISTIC MODELING OF INTERACTIONS BETWEEN MINERALS AND
ORGANICS IN CIVIL INFRASTRUCTURE MATERIALS

A Dissertation

by

JAVIER AURELIO GRAJALES SAAVEDRA

Submitted to the Office of Graduate and Professional Studies of
Texas A&M University
in partial fulfillment of the requirements for the degree of

DOCTOR OF PHILOSOPHY

Chair of Committee,	Dallas N. Little
Committee Members,	Lisa M. Pérez
	A. Paul Schwab
	Robert L. Lytton
	Youjun Deng
Head of Department,	Robin Autenrieth

May 2020

Major Subject: Civil Engineering

Copyright 2020 Javier Aurelio Grajales Saavedra

ABSTRACT

This document comprises a sum of research efforts aimed at the discovery of mechanisms of interaction between mineral (inorganic), and organic substances used or occurring in civil infrastructure materials. This endeavor involves the consideration of both physical and chemical phenomena as the driving forces of the interaction mechanisms. The scale required for such purpose magnifies the very specific chemical composition and structure of infrastructure materials: the molecular scale, because it is the molecular scale that which captures both the physical and chemical nature of all substances composing matter.

Within the various types of civil infrastructure materials and systems, this work focuses on those used for roadway pavements: asphalts, polymers, mineral fillers, aggregates, and soil minerals.

A substantial portion of the research efforts reported in this document is dedicated to the elucidation of mechanisms of interaction between asphalt molecular constituents and mineral fillers used in the mastic phase of asphalt mixtures. Specifically, one case has posed great interrogatives to many researchers due to its manifold advantages: hydrated lime. As opposed to other fillers, such as those of siliceous nature, hydrated lime has been experimentally proven to improve asphalt performance and durability and has been addressed as an “active filler” as opposed to the rest which have been named “inert fillers”. Yet, the molecular mechanism explaining such difference in behavior is still unclear.

With the advance of molecular modeling tools and techniques, this work shows the first insights into the molecular nature of the interaction of hydrated lime with key molecular species present in asphalt mixtures. The superiority of the interactions of hydrated lime with asphalt moieties is both validated and quantified by the determination of the molecular free energies of interaction of each component, and the formulation of a dissociation energy value.

In the case of the polymer interaction with soil minerals it is shown how experimentally a novel formulation can be synthesized, experimentally validated, and further evaluated using atomistic modeling techniques including molecular dynamics simulations to qualitatively verify trends and behaviors with representative soil minerals such as sodium montmorillonite.

DEDICATION

To my parents Teresa and Aurelio who have supported me ever since I was born and guided me through the path of both scientific and ethical learning in an integral way. This constitutes an invaluable inheritance I have been blessed with.

To my brother Francisco who has always been a source of encouragement, and who has shown with his actions throughout his life a righteous example to follow.

To my niece Melisabel who is the youngest hope of our family. In the simple, innocent, and sincere way children are she has always irradiated nothing but happiness and joy against moments of bitterness we adults often have.

ACKNOWLEDGEMENTS

I am grateful to my committee chair, Dr. Dallas Little, who gave me the invaluable opportunity of pursuing a Ph.D. degree throughout which his guidance and support was never absent, and who year after year never allowed the will to succeed to falter in me.

I would like to equally express my gratitude to Dr. Lisa Pérez and Dr. Paul Schwab for they have resiliently guided me through the endeavor of delving into the scientific field of chemistry and the laborious task of finding ways to apply the fundamental knowledge of this field to advance the state of the art and innovation in the civil engineering field.

I am thankful to Dr. Youjun Deng, and Dr. Robert Lytton for all the knowledge they imparted in me with great talent, and as well for their enthusiasm and support toward developing my research topic.

CONTRIBUTORS AND FUNDING SOURCES

Contributors

This work was supervised by a dissertation committee consisting of Professors Dallas. N. Little (advisor) and Robert L. Lytton of the Zachry Department of Civil and Environmental Engineering, Professors A. Paul Schwab and Youjun Deng of the Department of Soil and Crop Sciences, and Dr. Lisa Pérez Graduate Faculty of Texas A&M University and Associate Director for Enablement of the High Performance Research Computing (HPRC) center.

The Nuclear Magnetic Resonance (NMR) data analyzed for Chapter 4 was obtained by Professor Gregory Wylie of the NMR facility of the Department of Chemistry, as well the Neutron Activation Analysis (NAA) data in this same chapter was obtained by the staff of the Elemental Analysis Laboratory under the direction of Dr. Bryan Tomlin.

Funding Sources

This graduate study was supported in its entirety through a graduate research assistantship awarded by the Zachry Department of Civil and Environmental Engineering of Texas A&M University.

TABLE OF CONTENTS

	Page
ABSTRACT	II
DEDICATION	IV
ACKNOWLEDGEMENTS	V
CONTRIBUTORS AND FUNDING SOURCES.....	VI
TABLE OF CONTENTS	VII
LIST OF FIGURES.....	IX
LIST OF TABLES	XII
1. INTRODUCTION.....	1
1.1. Main objectives	2
1.2. Specific objectives.....	3
1.3. Research hypotheses	3
2. THEORETICAL BACKGROUND	4
2.1. Theoretical foundations of molecular modeling	4
2.1.1. Classical mechanics modeling.....	5
2.1.2. Quantum mechanics modeling	11
3. INTERACTIONS BETWEEN ASPHALT AND MINERAL FILLERS	24
3.1. The problem of carboxylic acids in asphalt	24
3.2. Classical mechanics modeling	25
3.2.1. Models of mineral fillers used in asphalt mixtures	25
3.2.2. Models of asphalt molecular species.....	26
3.2.3. Modeling methodology and parameters of interest.....	28
3.2.4. Results and discussion.....	39
3.3. Quantum mechanics modeling.....	41
3.3.1. Models of mineral fillers used in asphalt mixtures	41
3.3.2. Models of asphalt molecular building blocks.....	45
3.3.3. Modeling methodology and parameters of interest.....	46

3.3.4. Results and discussion.....	56
3.3.5. Agreement with experimental data.....	63
4. INTERACTIONS BETWEEN A TERPOLYMER AND SOIL MINERALS	64
4.1. Experimental synthesis procedure.....	64
4.1.1. Synthesis of the cationic co-polymer (stage 1)	65
4.1.2. Synthesis of the terpolymer via hydrolysis (stage 2)	66
4.2. Experimental validation techniques	67
4.2.1. Nuclear magnetic resonance (NMR).....	68
4.2.2. Neutron activation analysis (NAA).....	71
4.3. Insights from atomistic modeling.....	72
4.3.1. TPAM interactions with sodium montmorillonite	72
5. CONCLUSIONS	75
5.1. Asphalt and mineral filler systems	75
5.2. Terpolymer (TPAM) interaction with soil minerals	78
REFERENCES	80

LIST OF FIGURES

	Page
Figure 2.1. Changes in conformation and geometry for an acrylamide based repeating unit of a polymer before and after geometry optimization.	10
Figure 3.1. Periodic atomistic models of the unit cell structure of (a) hydrated lime, (b) quartz, and (c) calcite. Atom colors are green (Ca), yellow (Si), grey (C), red (O), and white (H)	26
Figure 3.2. Examples of atomistic structures with atom types and partial charges assigned: (a) an asphaltene, (b) a quartz unit cell. Each atom is labeled with a number (partial charge) and initials (atom type).....	29
Figure 3.3. Example of structural changes in an asphaltene molecule before (a) and after (b) geometry optimization.	30
Figure 3.4. Construction process for the asphalt supercell: (a) cell with reduced density of 0.1 g/cm ³ , (b) agglomeration, (c) cell equilibrated to a density of 0.9g/cm ³	32
Figure 3.5. Layered supercells constructed: (a) asphalt-quartz, (b) asphalt-calcite, (c) asphalt-hydrated lime. Atom colors are dark yellow (Si), green (Ca), red (O), white (H), grey (C), and bright yellow (S).....	34
Figure 3.6. Effect of atom types and partial charges on dangling atoms at the cleaved surface of the quartz-asphalt interface.	35
Figure 3.7. Graphical conceptualization of the interfacial energy components in equation (22).....	37
Figure 3.8. Conolly surface fields calculated for each system: (a) composite system, (b) asphalt only, (c) mineral only.	38
Figure 3.9. Summary of results obtained with classical molecular modeling: (a) interaction energies and (b) work of adhesion.....	40
Figure 3.10. (a) hydrated lime unit cell, (b) reduced unit cell, and (c) hydrated lime discrete molecular unit. Atom colors are green (Ca), red (O), white (H).....	42
Figure 3.11. (a) Unit cell of a quartz crystal, (b) Structure of pyrosilicic acid, the molecular surrogate chosen to mimic the behavior of quartz. Atom colors are yellow (Si), red (O), white (H).	43

Figure 3.12. (a) Unit cell of calcite, (b) calcium bicarbonate complex surrogate for calcite. Atom colors are green (Ca), grey (C), white (H), and red (O).....	44
Figure 3.13. Graphical depiction of a dissociation reaction: calcium oxalate dissociating into oxalic acid and hydrated lime. Atom colors are green (Ca), red (O), grey (C), and white (H).....	51
Figure 3.14. Graphical scheme of the reaction when a hydrated lime molecule (pH=12.45) is the mineral filler introduced in an aqueous system with pH=6.5, value at which oxalic acid has dissociated into the charged species oxalate and two hydroniums. Atom colors are green (Ca), red (O), grey (C), and white (H).....	54
Figure 3.15. Graphical scheme of the reaction when calcium bicarbonate (model for calcite) is the mineral filler introduced in an aqueous system with pH=6.5, value at which oxalic acid has dissociated into the charged species oxalate and two hydroniums. Atom colors are green (Ca), red (O), grey (C), and white (H).....	55
Figure 3.16. Comparison between dissociation energies in water vs. n-dodecane for hydrated lime and pyrosilicic acid.....	58
Figure 3.17. Comparison between dissociation energies in water vs. n-dodecane for an isolated Ca^{2+} ion.....	59
Figure 3.18. Dissociation energies of carboxylic acid complexes in presence of hydrated lime versus quartz in water as the solvent.	59
Figure 3.19. Dissociation energies of heterocyclic moieties in n-dodecane as the solvent. (pydn = pyridine, thio = thiophene, pyol = pyrrole)	60
Figure 3.20. Dissociation energies for hydrated lime, calcite, and quartz models (pH = 6.5).	61
Figure 3.21. Contour map of the Laplacian of the electron density for the calcium oxalate complex.....	62
Figure 3.22. Example of the contour map of the Laplacian of the electron density for a typical ionic bonding case between sodium and chloride.....	62
Figure 4.1. Synthesis of the cationic co-polymer AM:AMTAC.....	66
Figure 4.2. Synthesis of the terpolymer TPAM through hydrolysis with NaOH.....	67

Figure 4.3. NMR spectra validating the structure and composition of the synthesized terpolymer TPAM. (a) ^1H spectrum, (b) ^{13}C spectrum, (c) three-peak carbonyl area detail.....	70
Figure 4.4. Intramolecular interactions between the three different modules in a TPAM repeating unit.	72
Figure 4.5. MD simulation snapshots: (a) and (b) for 50 waters, (c) and (d) for 100 waters, (e) and (f) for 250 waters. Atom colors are red (O), cyan (H), yellow (Si), grey (C), blue (N), purple (Na), green (Mg), and teal (Al).....	74

LIST OF TABLES

	Page
Table 2.1. Classification of each of the force field terms included in equation (1).	7
Table 3.1. Summary of asphalt molecular species evaluated in this study according to the three component model by Greenfield ¹¹	27
Table 3.2. Molecular species investigated as surrogates of asphalt macromolecular moieties. Atom colors are red (O), grey (C), white (H), blue (N), and yellow (S).	46
Table 3.3. Matrix with dissociation energy values obtained for hydrated lime, Ca ²⁺ , and quartz models.	57
Table 3.4. Experimental data from Petersen validating the reactive nature of hydrated lime with asphalt ⁶	63
Table 4.1. TPAM chain structure and composition.....	68
Table 4.2. NAA results showing the sodium content in the TPAM samples analyzed....	71

1. INTRODUCTION

The central focus of this work is the determination of a modeling methodology capable of defining the chemical and physical mechanisms of interaction between minerals and organics in civil infrastructure materials at the atomistic scale. Specifically, this study seeks to find ways of defining the strength of the interactions between infrastructure materials at the atomistic scale, and the differentiation as to whether such interactions are of a physical (non-bonding) or chemical (bonding/reactive) nature. The systems of interest for this study are: the interaction of hydrated lime and other fillers with asphalt, and the interaction of a novel polymer formulation with soil minerals. The major modeling component of the investigation is focused on the asphalt-mineral filler interaction system. Whereas, for the case of the polymer formulation, most of the investigation focuses on the experimental synthesis procedures with a minor computational component.

The document is organized in three chapters. First, an introductory chapter of theoretical background. This chapter explains in depth the mathematical, physical, and chemical theory and postulates needed to better understand the foundations of the modeling methods (classical and quantum mechanics based).

The second chapter addresses the interaction of hydrated lime and other fillers with asphalt, which is subdivided into classical modeling and quantum atomistic modeling. This is the major contribution of the research work presented in this document. Throughout this chapter, the reader will be presented the advantages and

constraints of each modeling methodology (classical versus quantum mechanics based), and the reasons why results differ from one to another. Furthermore, it will be shown how the results of the quantum modeling segment of this chapter corroborate experimental findings on the interaction between hydrated lime and asphalt.

Finally, the third chapter addresses the interaction between a novel polymer formulation and soil minerals. In this chapter the major emphasis is placed on the experimental synthesis procedure and how the composition and structure of the newly formulated compound could be validated using elemental analysis techniques. Insights on the atomic structure and behavior of the polymer are obtained using classical molecular modeling methods as well as qualitative information about the interaction with soil minerals.

1.1. Main objectives

- The application of atomistic modeling methods and techniques as a methodology for the evaluation of interactions between minerals and organics in civil infrastructure materials.
- The establishment of a modeling methodology capable of distinguishing between chemical (reactive) interactions versus physical (non-bonding) interactions, and the impact of each on the behavior of materials.
- For the case of the interaction between hydrated lime and asphalt, this work seeks mechanistic evidence of the reactivity of hydrated lime as a filler in asphalts, as well as quantitative comparison between the strength of the interaction against other potentially reactive fillers such as calcite.

1.2. Specific objectives

- Obtain mechanistic evidence of the reactivity of hydrated lime as a filler in asphalts, as well as a quantitative comparison of the strength and character of the interaction mechanisms.
- Qualitative evidence of the behavior of the polymer that corroborates its ability to sorb interlayer cations as well as to sorb onto the surface of the mineral.

1.3. Research hypotheses

- Lime as a filler in asphalt:
 - Hydrated lime is able to form strong complexes with specific moieties such as carboxylic acids that are problematic to asphalt durability and performance.
- Polymer and sodium montmorillonite:
 - The polymer formulation is able to sorb the sodium interlayer cations present in montmorillonite.
 - The polymer formulation is capable of providing a hydrophobic barrier through sorption to the siloxane surface of the mineral.

2. THEORETICAL BACKGROUND

2.1. Theoretical foundations of molecular modeling

The following contents and subsections are a compilation of concepts and theoretical postulates gathered from three major sources addressing computational chemistry in general ^{1,2} and density functional theory (DFT) ³. The different concepts and equations are progressively explained in a fashion intended to provide a simplified, but comprehensive overview of the set of major theories that provide the physical and chemical foundations for the various existing molecular modeling techniques and methods.

The essential idea of molecular modeling is the representation of the chemical structure of substances in a three-dimensional geometrical space to account for both the physical and chemical properties of matter. Unlike modeling techniques at larger scales, such as continuum models, molecular modeling has the capability of capturing the properties of matter with the specificity inherent to its very elemental composition.

As the main idea is to explicitly represent the chemical structure of substances, molecular models often rely on physical the representation of atoms of the different elements as balls and bonds connecting these atoms as “sticks”. In this fashion, all kinds of chemical structures can be represented and understood in a simple way. This is known as the “ball and stick” model of the chemical structure of matter.

Although very useful and illustrative, this is just a model that gives a visual understanding of a given chemical structure. What the drawings do not show is the

actual physical and chemical numerical models that govern the behavior of the bonds and atoms. Nowadays, such numerical models are vast, but can be divided into two main categories: classical mechanics models and quantum mechanics models. As their names indicate, each category relies on a different set of mechanical foundations that provide a specific definition of what bonds and atoms are and their corresponding behavior restrained to a set of theoretical assumptions and limitations. The nuts and bolts of these two main categories will be explained in depth in the following sub-sections.

2.1.1. Classical mechanics modeling

Classical mechanics modeling is founded on a set of postulates including Newton's laws of motion, Coulomb's law, and Lennard-Jones equations to define a set of potentials that altogether describe the energy of a molecular system. The main mechanical assumption in classical mechanics modeling is the consideration of atoms as "balls" and bonds as "springs" whose movements respond to Hooke's law. That is, $F_s = -kx$, where the restoring force of the spring F_s is used as the definition of the attractive or repulsive nature of the chemical bonds. Because the potential energy is the parameter needed to unify an energy expression for the analysis of a molecular system, Hooke's law is derived to yield the potential energy stored in the bonds due to the mass of the atoms and their positions in and out of equilibrium as $V(x) = \frac{1}{2}kx^2$. Where $V(x)$ is the potential energy of the system as a function of the spatial coordinate x , and k is the "spring constant" specific to bonds formed between atoms of different elements. In this way, all the changes in energy due to the motions of atoms can be quantified in terms of

Hooke's law not only for linear displacement, but also for angular and torsional displacements. These three main modes of motion define what is called the "bonding" interactions between atoms representing covalent bonds in a numerical way.

Coulomb's law and Lennard-Jones equations in the classical mechanics modeling approach represent the "non-bonding" interactions between atoms of different elements. That is, the electrostatic attraction and repulsion forces and the short-range permanent or transient induced dipole moment forces: the van der Waals forces. Together with Hooke's law, Coulomb's law and Lennard-Jones equations provide a complete definition of the behavior of atoms. This is because atoms and their bonds are described by an electronic structure dependent upon the number and way electrons are shared or donated. By assigning an explicit geometrical entity to an atom (a sphere), the entire set of equations (mechanical, electrostatic, and short-range induced dipole moment) can be coupled into one expression and parametrized for almost every single element of the periodic table. This cannot be achieved using other techniques such as continuum modeling. Such coupled energy expression is the single most important and definitive component of the classical molecular modeling method. Therefore, it has a specific denomination: a force field.

2.1.1.1. Force fields and their characteristics

In classical molecular mechanics, a force field is the coupled energy expression mathematically defining all the components of energy necessary to quantify both the mechanical and electrical behavior of a substance composed of a given set of chemical elements. Several degrees of complexity can be formulated in a force field. Therefore,

there are three classes (I, II and III), the simplest being a force field class I as in equation (1).

$$V = \frac{k}{2}(r - r_0)^2 + \frac{k}{2}(\theta - \theta_0)^2 + \frac{1}{2} \sum_j \{B_j(1 - d_j \cos[n_j \varphi])\} + \frac{k}{2} \omega_{av}^2 + \frac{q_i q_j}{4\pi \epsilon_0 \epsilon_r r_{ij}} + \epsilon_{ij} \left[2 \left(\frac{r_{ij}^0}{r_{ij}} \right)^9 - 3 \left(\frac{r_{ij}^0}{r_{ij}} \right)^6 \right] \quad (1)$$

As can be noted in equation (1), the first four terms are defining mechanical energy, whereas the two last ones are Coulomb's law (for electrostatic energy) and Lennard-Jones equation for induced dipole moment (van der Waals) energy. Together, the six terms provide a comprehensive definition of the behavior of an atom. **Table 2.1** provides the classification of each of the six terms in equation (1).

Table 2.1. Classification of each of the force field terms included in equation (1).

Class I Force Field	
Bonded terms (covalent bonds)	
Bond stretch	$V = \frac{k}{2}(r - r_0)^2$
Angle bend	$V = \frac{k}{2}(\theta - \theta_0)^2$
Torsion	$V = \frac{1}{2} \sum_j \{B_j(1 - d_j \cos[n_j \varphi])\}$
Inversion	$V = \frac{k}{2} \omega_{av}^2$
Non-bonded terms (electrostatic and van der Waals)	
Electrostatic	$V = \frac{q_i q_j}{4\pi \epsilon_0 \epsilon_r r_{ij}}$
van der Waals	$V(r) = \epsilon_{ij} \left[2 \left(\frac{r_{ij}^0}{r_{ij}} \right)^9 - 3 \left(\frac{r_{ij}^0}{r_{ij}} \right)^6 \right]$

As mentioned before, the six terms in **Table 2.1** correspond to a class I force field providing a fairly complete definition of the possible interactions an atom can have. However, complex systems may require more specialized expressions. For this reason, force fields have been developed accounting for a larger set of parameters and coefficients. An example is the COMPASSII force field (class III) ⁴, where additional constants are added to a single term, and as well additional terms are defined for combined energy components. All these contribute to a richer definition of the interatomic energies and modes of motion in three dimensions.

Finally, an important aspect of force fields is that their coefficients are parametrized for each specific elemental entity composing a molecular species. Many force fields are very complete in terms of the list of species they can handle. However, this might become a limitation at some point if the species in study is not well parametrized in the force field chosen.

2.1.1.2. Types of calculations

Three main types of calculations are performed in classical mechanics modeling. These are: single point energy (SPE), geometry optimization (or energy minimization), and molecular dynamics.

2.1.1.2.1. Single point energy (SPE)

The simplest and most basic calculation is the single point energy (SPE). In this type of calculation, for a desired molecular geometry that is fixed, a single point on the potential energy surface (PES) is calculated based on a given force field expression. An important concept is that of the potential energy surface (PES), which is particular to

every molecule. The potential energy surface (PES) is the two-dimensional energy plane that is defined by the different geometrical states a molecule can occupy depending upon the number of coordinates that can vary. For example, in the case of water (H_2O), there are two coordinates that dictate the shape of the potential energy surface: the angle between the hydrogens and oxygen atom, and the linear distance between the hydrogen and oxygen bonds (O-H). Depending on the geometrical state that a water molecule may occupy, different potential energy values will be obtained, some higher than others, and there will also be a minimum which corresponds to the most favorable state in which the molecule will exist.

2.1.1.2.2. Geometry optimization

Molecular geometries are commonly represented with idealized conformations, which may not be the true minimum energy geometry. The geometry optimization calculation is that which allows finding the minimum locus in the potential energy surface. In this type of calculation, bonds between atoms in a molecule are relaxed, and intra- and inter-molecular forces are minimized to reach a minimum in value energy. Geometry optimization calculations are highly dependent on the initial structure defined. Depending on the initial structure, a local minimum may be found instead of a global minimum. Therefore, care must be taken as to provide a reasonable guess for the initial structure of the molecule in study. As an example, **Figure 2.1** shows the initial structure defined for an acrylamide based repeating unit of a polymer, and its corresponding optimized structure. Significant changes can be observed, such as changes in orientation

of several atoms as well as changes in interatomic distances dictating attraction between certain atom groups.

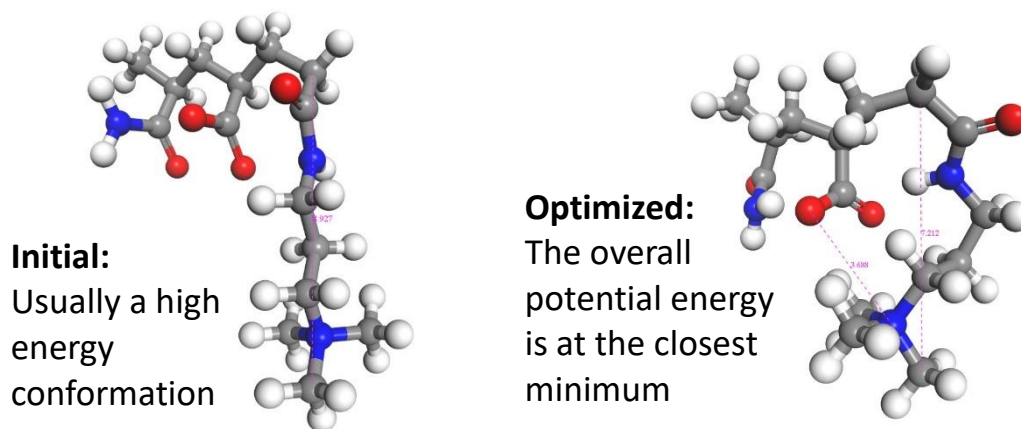


Figure 2.1. Changes in conformation and geometry for an acrylamide based repeating unit of a polymer before and after geometry optimization.

2.1.1.2.3. *Molecular dynamics*

Classical molecular dynamics is the most complex type of calculation in classical molecular modeling. Molecular dynamics is a simulation technique to calculate the motions of molecular systems and their evolution in time based on defined interatomic potentials. The physical basis for molecular dynamics simulation is Newton's second law of motion, as defined in equation (2).

$$F(r) = -\frac{\partial V}{\partial r_i} = m \frac{\partial^2 r}{\partial t^2} \quad (2)$$

In a molecular dynamics simulation the second order differential equation in equation (2) is solved iteratively with algorithms based on mathematical series (Taylor's expansion series). A popular algorithm developed is the Verlet algorithm. Such iterative

process is repeated for every time step of the molecular dynamics simulation to obtain the potential energy value corresponding to that time step.

Several important constraints can be specified in a molecular dynamics simulation. Within those, fundamental thermodynamic variables such as temperature and pressure can be specified. Based upon the thermodynamic variables considered, different thermodynamic ensembles exist. The three ensembles more widely used are: the NPT, NVT, and NVE. Where, NPT stands for constant number of molecules (N), constant pressure (P), and constant temperature (T); NVT stands for constant number of molecules (N), constant volume (V), and constant temperature (T); and finally NVE stands for constant number of molecules (N), constant volume (V), and constant enthalpy (E).

2.1.2. Quantum mechanics modeling

The major limitation of classical mechanics modeling is the inability of the modeling approach to account for chemical reactions. In classical mechanics modeling, interatomic potentials do define bonded and non-bonded interactions between atoms, but only under the condition that no bonds are broken or reformed. Quantum mechanics modeling overcomes this important limitation by incorporating the electronic structure of atoms into the mathematical expressions governing the modeling approach. This, however, has consequences when using quantum mechanics modeling: limited number of atoms in a system and higher computational costs and times of computation. Despite these consequences, quantum mechanics modeling is the only way in which reactivity can be truly assessed in a molecular system, which in many cases is needed to describe

specific phenomena. The physical basis for quantum mechanics based modeling originates from Schrödinger's equation.

2.1.2.1. Schrödinger's equation

Quantum mechanics modeling involves the determination of the electronic structure of matter, which in turn involves knowing where electrons are located in a given molecular system. The postulate that defines the location of electrons in a physical system and their corresponding energy levels is Schrödinger's equation, formulated as follows in equation (3):

$$-\frac{\hbar^2}{2m} \sum_{i=1}^N \nabla^2 \psi + \sum_{i=1}^N V \psi = E \psi \quad (3)$$

Even though a valid and important postulate, an exact solution for Schrödinger's equation has been found only for a single hydrogen atom. For any other of the larger atoms, only approximate solutions exist. Furthermore, when trying to solve for a single small molecule, a major numerical complication unfolds. For example, carbon dioxide CO₂ has a total of 22 electrons, which means Schrödinger's equation is a 66 dimensional function (3 dimensions per electron)³. This is denominated a many-body problem, and it becomes very difficult to solve. In lieu of this major complexity, simplified quantum theories have been developed. These incorporate specific theoretical postulates that allow a simplified solution. All these quantum theories have been grouped and categorized in three major levels, from the most complex to the least complex: *ab initio*, density functional theory (DFT), and semi-empirical. Within the scope of this work only density functional theory (DFT) will be explained.

2.1.2.2. Density functional theory (DFT)

Density functional theory is a quantum mechanical technique formulated to calculate atomic properties and molecular reactions based upon the definition of the electron density function $\rho(\mathbf{r})$. The electron density function $\rho(\mathbf{r})$ is defined as the probability that an electron in an individual wavefunction $\psi_i(\mathbf{r})$ is located at the position vector \mathbf{r} with spatial coordinates x , y , and z . The previous statement is the single most important simplification of DFT as a quantum mechanical technique, and it is that $\rho(\mathbf{r})$ is a function of only three spatial coordinates as opposed to the full wavefunction solution of Schrödinger's equation. Mathematically $\rho(\mathbf{r})$ is formulated then as in equation (4):

$$\rho(\mathbf{r}) = 2 \sum_i \psi_i^*(\mathbf{r})\psi_i(\mathbf{r}) = 2|\psi_i(\mathbf{r})|^2 \quad (4)$$

Having defined and formulated the electron density function as the prime theoretical foundation, according to DFT then, the energy of a given system is formulated as a “functional” of the electron density function. Hence the name “density functional theory”, where a functional is defined as a function whose argument is another function. The ground state energy of a system is formulated as in equation (5):

$$E_0[\rho(\mathbf{r})] \quad (5)$$

Such a formulation is called the 1st DFT theorem by Hohenberg and Kohn: the existence theorem; and it reads as follows: *the ground-state energy from Schrödinger's equation is a unique functional of the electron density*³. In other words, the ground-state electron density uniquely determines all properties, including the energy and the

wavefunction of the ground state. Furthermore, the 2nd DFT theorem, the variational theorem, by Hohenberg and Kohn reads as follows: *any trial electron density function will give an energy higher than or equal to the true ground state energy, and the electron density that minimizes the energy of the overall functional is the true electron density corresponding to the full solution of the Schrödinger equation*¹⁻³. This theorem is formulated as in equation (6):

$$E_v[\rho_t(\mathbf{r})] \geq E_0[\rho_0(\mathbf{r})] \quad (6)$$

With these two theorems DFT has the potential to find the true total energy of a molecular system, but so far it does not define what the functional is, nor provide means of how to find such energy. Such means were formulated by Kohn and Sham in 1965, setting their foundation in two basic ideas.

First, Kohn and Sham divided the energy functional expression into non-interacting electron terms and interacting electron correction terms. These are formulated as follows in equation (7)¹:

$$E[\rho(\mathbf{r})] = T_{ni}[\rho(\mathbf{r})] + V_{ne}[\rho(\mathbf{r})] + V_{ee}[\rho(\mathbf{r})] + \Delta T[\rho(\mathbf{r})] + \Delta V_{ee}[\rho(\mathbf{r})]$$

Where,

$$T_{ni}[\rho(\mathbf{r})] = \text{non-interacting electron kinetic energy} \quad (7)$$

$$V_{ne}[\rho(\mathbf{r})] = \text{nuclear-electron interaction potential}$$

$$V_{ee}[\rho(\mathbf{r})] = \text{classical electron-electron repulsion potential}$$

$$\Delta T[\rho(\mathbf{r})] = \text{kinetic correction term for interactive nature of electrons}$$

$$\Delta V_{ee}[\rho(\mathbf{r})] = \text{potential correction term for non-classical electron interactions}$$

The first three terms formulated in equation (7) are “known” or can be determined exactly. However, the last two terms pose a challenge as they are

“unknown”. So much more complex is their determination that their sum was attributed a special denomination: the exchange correlation functional E_{XC} , formulated then as follows in equation (8):

$$E_{XC} = \Delta T[\rho(\mathbf{r})] + \Delta V_{ee}[\rho(\mathbf{r})] \quad (8)$$

The physical meaning of such partitioning of energy functionals rests on a key idea Kohn and Sham defined which is the concept of a hypothetical noninteracting reference system in which the ground state electron density distribution is the same as in the real ground state system $\rho_r = \rho_0$. The ground state **electronic** energy of the real system is defined then as in equation (9) ²:

$$E_0 = \langle T[\rho_0] \rangle + \langle V_{Ne}[\rho_0] \rangle + \langle V_{ee}[\rho_0] \rangle \quad (9)$$

Where $T[\rho_0]$ is the electron kinetic energy functional, $V_{Ne}[\rho_0]$ is the nucleus-electron attraction potential energy functional, and $V_{ee}[\rho_0]$ is the electron-electron repulsion potential energy functional. The major problem to be able to use this equation is the fact that the terms $T[\rho_0]$ and $V_{ee}[\rho_0]$ are simply **not known** ². However, by employing the idea of the hypothetical reference system of noninteracting electrons, a term can be defined as the deviation of the real electronic kinetic energy from that of the reference system as follows in equation (10) ²:

$$\Delta \langle T[\rho_0] \rangle = \langle T[\rho_0] \rangle_{real} - \langle T[\rho_0] \rangle_{reference} \quad (10)$$

Same as with the electronic kinetic energy, a deviation of the real electron-electron repulsion energy from a reference classical nonquantum cloud of negative charge is defined as in equation (11) ²:

$$\Delta \langle V_{ee} [\rho_0] \rangle = \langle V_{ee} [\rho_0] \rangle_{real} - \langle V_{ee} [\rho_0] \rangle_{reference} \quad (11)$$

Where $\langle V_{ee} [\rho_0] \rangle_{reference}$ is defined according to classical electrostatic energy theory as the summation of the repulsion energies for pairs of infinitesimal volume elements formulated as in equation (12):

$$\langle V_{ee} [\rho_0] \rangle_{reference} = \frac{1}{2} \iint \frac{\rho_0(\mathbf{r}_1)\rho_0(\mathbf{r}_2)}{r_{12}} d\mathbf{r}_1 d\mathbf{r}_2 \quad (12)$$

Having the defined the deviation terms, the total electronic energy equation for the real system can be expressed then as in equation (13):

$$E_0 = \Delta \langle T [\rho_0] \rangle + \langle T [\rho_0] \rangle_{reference} + \langle V_{Ne} [\rho_0] \rangle + \Delta \langle V_{ee} [\rho_0] \rangle + \langle V_{ee} [\rho_0] \rangle_{reference} \quad (13)$$

Substituting then the known terms and reordering (13) leads to equation (14):

$$E_0 = \langle T [\rho_0] \rangle_{reference} + \int \rho_0(\mathbf{r})v(\mathbf{r})d\mathbf{r} + \frac{1}{2} \iint \frac{\rho_0(\mathbf{r}_1)\rho_0(\mathbf{r}_2)}{r_{12}} d\mathbf{r}_1 d\mathbf{r}_2 + \Delta \langle T [\rho_0] \rangle + \Delta \langle V_{ee} [\rho_0] \rangle \quad (14)$$

Where the **exchange-correlation functional** E_{xc} previously introduced appears clearly defined in the last two terms of equation (14).

The first term in equation (14), $\langle T [\rho_0] \rangle_{reference}$, is the electronic kinetic energy of the noninteracting-electrons reference system, and since they are **noninteracting**, such electronic kinetic energy expression corresponds to the expectation value of the sum of

the one-electron kinetic energy operators over the ground state multielectron wavefunction of the reference system. Under these noninteracting conditions, the wavefunction of the reference system can be written exactly (for a closed-shell system)² as a single Slater determinant of occupied spin molecular orbitals, and therefore expressed in terms of spatial KS (Kohn-Sham) orbitals ψ_i^{KS} as equation (15):

$$\langle T[\rho_0] \rangle_{reference} = -\frac{1}{2} \sum_i^{2n} \langle \psi_i^{KS}(n) | \nabla_i^2 | \psi_i^{KS}(n) \rangle \quad (15)$$

The Kohn-Sham energy expression can be finally outlined as equation (16):

$$\begin{aligned} E_0 = & -\frac{1}{2} \sum_i^{2n} \langle \psi_i^{KS}(n) | \nabla_i^2 | \psi_i^{KS}(n) \rangle - \sum_{nucleiA} Z_A \int \frac{\rho_0(\mathbf{r}_1)}{\mathbf{r}_{1A}} d\mathbf{r}_1 \\ & + \frac{1}{2} \iint \frac{\rho_0(\mathbf{r}_1)\rho_0(\mathbf{r}_2)}{\mathbf{r}_{12}} d\mathbf{r}_1 d\mathbf{r}_2 + E_{xc}[\rho_0] \end{aligned} \quad (16)$$

Equation (16) above clearly defines all the terms inherent to the ground state electronic energy, and it has devised a physically reasonable substitution method to single out all electron interaction effects into deviation terms that comprise the exchange-correlation functional, but it still does not define the exchange-correlation functional E_{xc} . At this point, it is time to introduce the second major basic idea by Kohn and Sham.

Kohn and Sham devised a method to solve the problem of finding the minimum energy solutions of the total energy functional by demonstrating that first, a single individual electron equation could be used to find the right electron density. Such equation, called the ‘‘Kohn-Sham (KS) equation’’ is obtained by differentiating the energy expression with respect to the KS molecular orbitals. This, still using the fact that

the electron density distribution of the reference system is the same as that of the ground state of the real system, and is expressed as in equation (17):

$$\rho_0 = \rho_r = 2 \sum_i^{2n} |\psi_i^{KS}(n)|^2 \quad (17)$$

Substituting the electron density in terms of orbitals into the total energy expression in equation (16), and differentiating to vary E_0 with respect to the KS spatial orbitals leads to the Kohn-Sham equation (18):

$$\left[-\frac{1}{2} \nabla_i^2 - \sum_{\text{nuclei } A} \frac{Z_A}{|\mathbf{r}_{1A}|} + \int \frac{\rho(\mathbf{r}_2)}{|\mathbf{r}_{12}|} d\mathbf{r}_2 + v_{XC}(n) \right] \psi_i^{KS}(n) = \varepsilon_i^{KS} \psi_i^{KS}(n) \quad (18)$$

Where ε_i^{KS} are the Kohn-Sham energy levels, and $v_{XC}(n)$ is the exchange correlation potential, which is a functional derivative of the exchange correlation energy $E_{XC}[\rho(\mathbf{r})]$. The exchange correlation potential can thus be obtained via functional differentiation as in equation (19):

$$v_{XC}(n) = \frac{\delta E_{XC}[\rho(\mathbf{r})]}{\delta \rho(\mathbf{r})} \quad (19)$$

The expression in brackets in equation (18) has been denominated as the Kohn-Sham operator, h^{KS} . Therefore, the Kohn-Sham equation reduces to:

$$h^{KS}(n) \psi_i^{KS}(n) = \varepsilon_i^{KS} \psi_i^{KS}(n) \quad (20)$$

Kohn-Sham equation has great similarity to Schrödinger equation, but the major difference is that the Kohn-Sham equation lacks the summation operators appearing in the full Schrödinger equation, meaning that the solution to the Kohn-Sham equation is a single-electron wavefunction that depends only on three spatial variables³.

Still, at this point, there are two caveats to keep in mind to solve the Kohn-Sham equation: the electron density function $\rho_0(\mathbf{r})$ is not known, and the exchange correlation energy functional $E_{xc}[\rho_0]$ is still not known.

Finally, the way in which Kohn and Sham circumvented this problem is by developing an iterative method, which is the central part of their second basic idea: to use an initial estimation of the electron density in the KS equations, to then calculate and initial estimation of the KS orbitals and energy levels; this initial estimation is then used to iteratively refine the orbitals and energy levels, and the final KS orbitals are used to calculate an electron density that in turn is used to calculate the final true energy. Better explained in a condensed list of steps, the process goes as:

1. Define an initial, trial electron density.
2. Solve the Kohn-Sham equations defined using the trial electron density to find the single-electron KS orbitals and energy levels.
3. Calculate the electron density defined by the newly calculated KS orbitals and energy levels in step 2.
4. Compare the calculated electron density with the initial trial electron density. If the two densities are the same, then this is the true ground-state electron density, and it can be used to compute the true total electronic energy of the system. If the two densities are different, then the trial electron density must be updated and the process repeats again from the second step.

Following these simplified and condensed steps it can be noted that Kohn and Sham formulated an iterative method that is *self-consistent*. The details of the steps to their solution are given below.

The standard strategy for solving the KS equations is (as in other quantum mechanical methods such as Hartree-Fock) to expand the KS orbitals in terms of basis functions ϕ . In fact, the same basis functions are often used as in wavefunction based methods. Thus, the expansion is formulated as follows in equation (21):

$$\psi_i^{KS} = \sum_{s=1}^m c_{si} \phi_s \quad i = 1, 2, 3, \dots, m \quad (21)$$

Substituting the basis set expansion into the KS equations leads to m sets of equations, each set with m equations, which can all be summed into a single matrix equation. The key to solving the KS equations then becomes the calculation of the matrix elements and the diagonalization of the matrix.

As previously outlined in a general fashion, a DFT calculation will start with an estimation of the electron density function $\rho(\mathbf{r})$ since this is needed to obtain an explicit expression for the KS operator h^{KS} . The first approximation usually assumes a noninteracting atom, obtained by summing mathematically the electron densities of the individual atoms of the molecule, at the starting molecular geometry specified. The KS matrix elements defined as $h_{rs} = \left\langle \phi_r \left| h^{KS} \right| \phi_s \right\rangle$ are calculated and the KS matrix is orthogonalized and diagonalized to give initial guesses of the coefficients c in the basis set expansion equation. These coefficients c are then used to calculate a set of KS

molecular orbitals which then are used to calculate a better electron density function ρ . This new density function is used to calculate improved matrix elements h_{rs} which in turn give improved coefficients c and then an improved density function. This iterative process is continued until the electron density converges. Then the final electron density and KS orbitals are used to calculate the energy. One major caveat needs to be identified at this point: the KS matrix elements are integrals over the basis functions, and because the functionals are so complicated, specifically the one dealing with the exchange-correlation potential $\langle \phi_r | v_{xc} | \phi_s \rangle$, the integrals can not be solved analytically. Thus, the only choice is to approximate the integral by summing the integrand in steps determined by a *grid*. Such grid, for example, for a DFT function $f(x, y, z)$ would specify the steps of x , y , and z . The finer the grid the greater the chance that accurate integrals are approximated.

Although the exchange-correlation potential v_{xc} has been defined explicitly, its calculation has not been addressed. As defined previously, the exchange-correlation potential is the functional derivative of the exchange-correlation energy functional $E_{xc}[\rho(\mathbf{r})]$, which in turn is a functional of the electron density function $\rho(\mathbf{r})$. Devising functionals $E_{xc}[\rho(\mathbf{r})]$ is the main problem in density functional theory, for all the theoretical difficulties of the Kohn-Sham DFT approach have been lumped into the functional. Approximation methods exist to define $E_{xc}[\rho(\mathbf{r})]$. Some of these, in order of sophistication are: local density approximation (LDA), generalized gradient approximation (GGA), meta-GGA (τ GGA), hybrid GGA, and hybrid meta-GGA. From

this point onwards, the word “functional” will refer specifically to E_{xc} according to a given approximation chosen for a given DFT calculation. As it is not the scope of this theoretical framework to delve into deep DFT functional algorithm development, the main characteristics of the different approximation methods listed above will be discussed briefly in the following subsections.

2.1.2.2.1. Local density approximation (LDA)

LDA is the simplest approximation to find E_{xc} . LDA considers only the electron density function in the “immediate vicinity”, meaning the region within an infinitesimal distance beyond a point. LDA is based on the assumption that at every point in the molecule the energy density (energy per electron) has the value that would be given by a homogeneous electron gas which had the same electron density at that point.

2.1.2.2.2. Generalized gradient approximation (GGA)

The GGA utilizes both the electron density and the gradient of the electron density with respect to the position vector, $\nabla\rho = \rho\left(\frac{\partial}{\partial x} + \frac{\partial}{\partial y} + \frac{\partial}{\partial z}\right)$.

2.1.2.2.3. Meta-GGA (τ GGA)

The meta-GGA based functionals further include more refinement by invoking the Laplacian of the electron density $\nabla^2\rho = \rho\left(\frac{\partial^2}{\partial x^2} + \frac{\partial^2}{\partial y^2} + \frac{\partial^2}{\partial z^2}\right)$

2.1.2.2.4. Hybrid GGA

The hybrid GGA functionals include an energy contribution from Hartree–Fock type electron exchange, calculated from the Kohn–Sham wavefunction of the

noninteracting electrons. Based on this, the exchange-correlation energy E_{xc} can be taken as a weighted sum of the DFT exchange-correlation energy and the Hartree–Fock exchange energy. Therefore, they contain the correction energy to the classical coulomb repulsion. Where, one main variation within this type of functionals is the percentage of Hartree–Fock exchange energy to use given that GGA functionals tend to underestimate barriers and Hartree–Fock methods tend to overestimate them. An example of a popular hybrid GGA functional is the B3LYP functional, which can be considered as an efficient exploratory option for the average quantum chemistry problem.

2.1.2.2.5. Hybrid meta-GGA

These functionals are meta-GGA functionals to which the Hartree–Fock exchange has been added.

3. INTERACTIONS BETWEEN ASPHALT AND MINERAL FILLERS

In this segment of the study an investigation is presented on the interactions of asphalt with mineral fillers at the atomistic scale. Mineral fillers play an important role in asphalt mixtures as they are the principal constituent of the mastic phase of the mixture. That is, the interfacial phase surrounding the stone aggregates in-between the pure asphalt coating phases. The mastic phase plays an important role in controlling the asphalt-aggregate performance providing increased adhesion and traction against slippage of one aggregate against the other. Furthermore, the mastic phase also plays an important role in the prevention of moisture damage as it is the fine organo-mineral interstitial matrix that acts as a barrier against water intrusion through the large aggregate skeleton of the asphalt mixture. For this reason, a strong physical and chemical interaction between the asphalt and the mineral filler is highly desired as it will create a better barrier against moisture intrusion and detrimental environmental factors. Mineral fillers are designated as either inert (non-reactive) or active (reactive). The latter case has been experimentally validated for hydrated lime⁵⁻⁷, whereas other fillers such as quartz have been found to be inert. Even though conclusive evidence suggest that hydrated lime reacts with asphalt molecular constituents, a predictive explanation of the reaction mechanism is still unclear.

3.1. The problem of carboxylic acids in asphalt

The presence of carboxylic acids in asphalt is problematic to the long-term durability of the asphalt mixture material used in pavement structures. Water is capable

of disrupting the interaction between the carboxylic group in asphalt moieties and several mineral aggregate surfaces ⁸. A typical example of this is the interaction between Si-OH groups in siliceous aggregates and a carboxylic acid moiety in asphalt, where the hydrogen bond formed can easily be broken by water.

Experimental evidence indicates that when hydrated lime is added to asphalt it is able to react almost selectively with the carboxylic acids in the asphalt forming complexes of $\text{Ca}-(\text{RCOO})_2$ that have been deemed as insoluble organic salts ⁷. Once the majority of the carboxylic acids have been complexed by the calcium ions released or present in the hydrated lime, stronger bonds can be achieved between these salts and other moieties with the aggregate surfaces. For this reason, this study aims to validate such experimental observations of the reactions between carboxylic acids and hydrated lime, as well as the development of a methodology to elucidate and predict the chemical mechanisms of interaction.

The following sections of this chapter focus on an atomistic modeling assessment of the interactions between key asphalt model moieties (including carboxylic acids among others) with three different mineral fillers (hydrated lime, calcite, and quartz) using both classical and quantum mechanics modeling approaches.

3.2. Classical mechanics modeling

3.2.1. Models of mineral fillers used in asphalt mixtures

The mineral models used for classical molecular modeling consist of periodic systems, which are the appropriate representation for crystalline species. In this study, models were gathered from the American Mineralogist Crystal Structure Database

(AMCSD)⁹. **Figure 3.1** illustrates the periodic unit cell models for the three mineral fillers investigated in this study: (a) hydrated lime, (b) quartz, and (c) calcite. From these unit cell models, supercells were constructed with the purpose of creating interfacial systems with the asphalt phase.

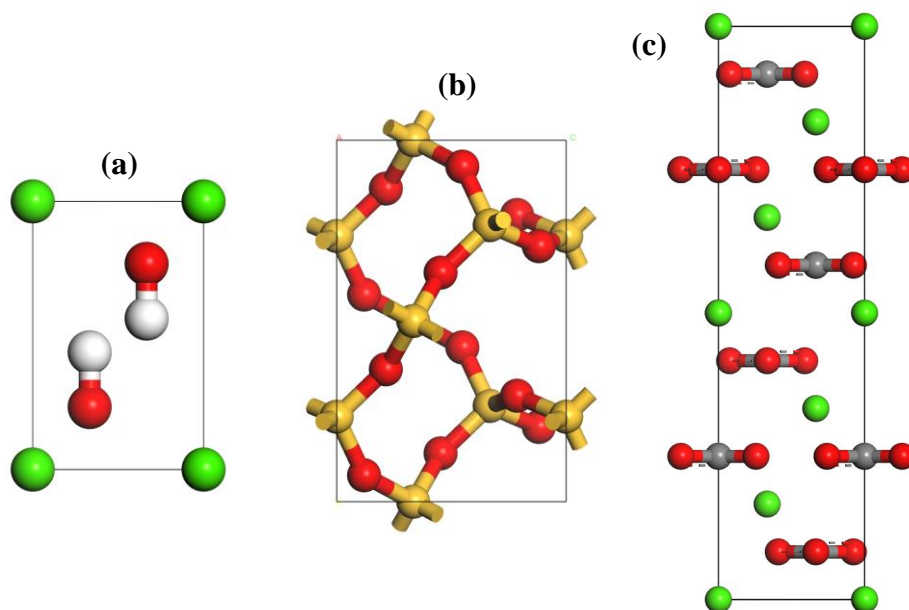


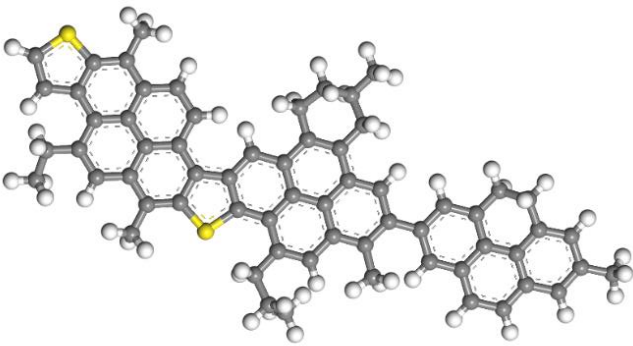
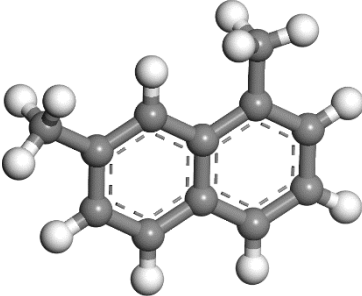
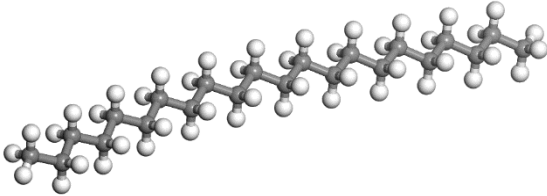
Figure 3.1. Periodic atomistic models of the unit cell structure of (a) hydrated lime, (b) quartz, and (c) calcite. Atom colors are green (Ca), yellow (Si), grey (C), red (O), and white (H)

3.2.2. Models of asphalt molecular species

Due to the complex diversity of organic chemical species in asphalt, creating an accurate atomistic representation becomes a challenge. Several models have been developed in the literature, some more complex than others. For example, Greenfield developed both a twelve-component model¹⁰, and a simpler three-component model of asphalt¹¹. In this study, the simpler three component model was chosen since the focus is to have a relative comparison of the interfacial behavior with mineral fillers rather

than exact determination of asphalt properties from molecular simulations. Such three-component model proposes two different asphalt compositions of which only one was chosen for creating an asphalt supercell consisting of: 5 asphaltenes containing sulfur as the only heteroatom; 27 1,7-dimethylnaphthalene; and 41 n-docosane (n-C₂₂) molecules. **Table 3.1** summarizes the structure, composition, and ratios of these molecules in the supercell.

Table 3.1. Summary of asphalt molecular species evaluated in this study according to the three component model by Greenfield ¹¹.

Species	#	Structure and composition. Atom colors are grey (C), white (H), and yellow (S).
Asphaltenes	5	
1,7-dimethylnaphthalene	27	
n-docosane	41	

3.2.3. Modeling methodology and parameters of interest

Prior to creating a supercell for the asphalt and mineral phases, specifying some general computational details is necessary.

3.2.3.1. General computational details

As explained in the theoretical background, classical mechanics modeling involves the formulation of a set of interatomic potentials according to theoretical postulates that together conform a coupled energy expression denominated a force field. The choice of an adequate force field is perhaps the most important decision in a classical simulation because the force field is the driving rule for the atoms defined in the system. If certain atom combinations are not properly defined in the force field chosen, the calculation will fail. In this study, the choice of a force field was not a straightforward decision because force fields are designed to handle either organic species or mineral inorganic species separately; and in the case of this study, the central aim is to evaluate an organo-mineral interface. For this reason, a search had to be launched to find a force field that could handle both mineral and organic species together. Such a force field was discovered: the INTERFACE force field¹². Another reason why the INTERFACE force field was a convenient choice is the flexibility of modifying parameters such as the partial charges for certain atom types. Other force fields that are of a commercial nature such as the COMPASSII force field cannot be modified. Having the appropriate force field available made the idea of the classical simulation feasible. However, the other major requirement in a classical calculation is to be able to have an accompanying compatible force field driver. The force field driver is the software that is

capable of handling the force field and employing its mathematical rules, and parameters into a given calculation. For the case of this study, the most practical choice compatible with the INTERFACE force field was the Materials Studio suite.

3.2.3.2. Model preparation and supercell construction

Having defined the essential computational details, the next step is to prepare the atomistic models for the simulations. This process is summarized in three steps:

1. Construct reasonable atomistic structures for the phases in study (such as those shown in **Table 3.1**)
2. Assign atom types and calculate partial charges as specified by the force field chosen
3. Geometry optimize the individual structures and construct the supercells that represent each of the phases in study.

Step 2 is critical because without assigning the correct atom types and/or partial charges, the force field will not perform properly. Examples of two structures (a quartz

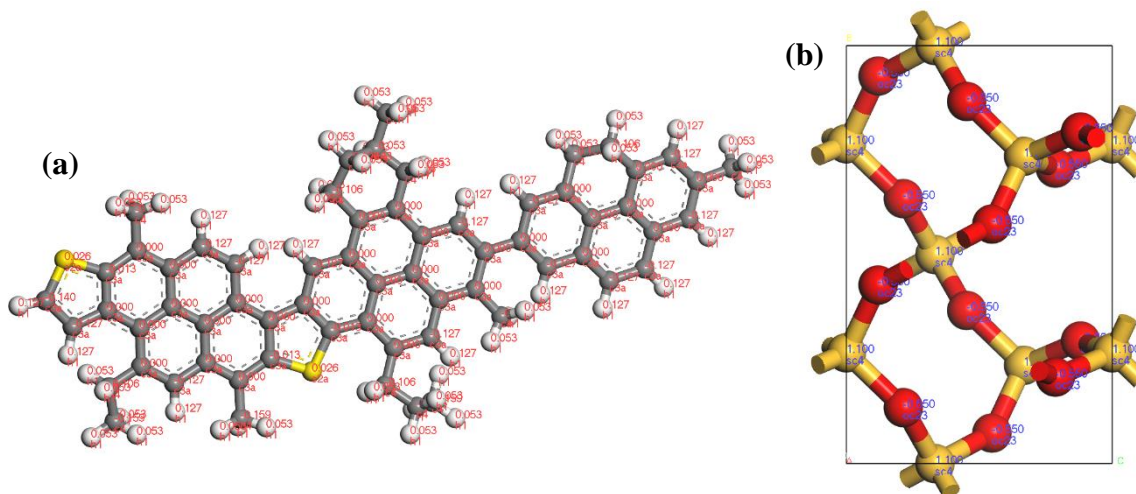


Figure 3.2. Examples of atomistic structures with atom types and partial charges assigned: (a) an asphaltene, (b) a quartz unit cell. Each atom is labeled with a number (partial charge) and initials (atom type).

unit cell and an asphaltene) with assigned force field types and partial charges are shown in **Figure 3.2(a)** and **(b)**.

Step 3 is important for facilitating the supercell construction process. Even though upon construction the structures are optimized, starting from the best (minimum energy) conformation possible is preferred. **Figure 3.3(a)** and **(b)** is an example of the asphaltene model optimized, illustrating how the geometry changes as a portion of the polycyclic aromatic structure rotates to a staggered orientation.

Once the structures are optimized, the supercell construction process can be started. For the case of an asphalt supercell this process is not entirely automatic.

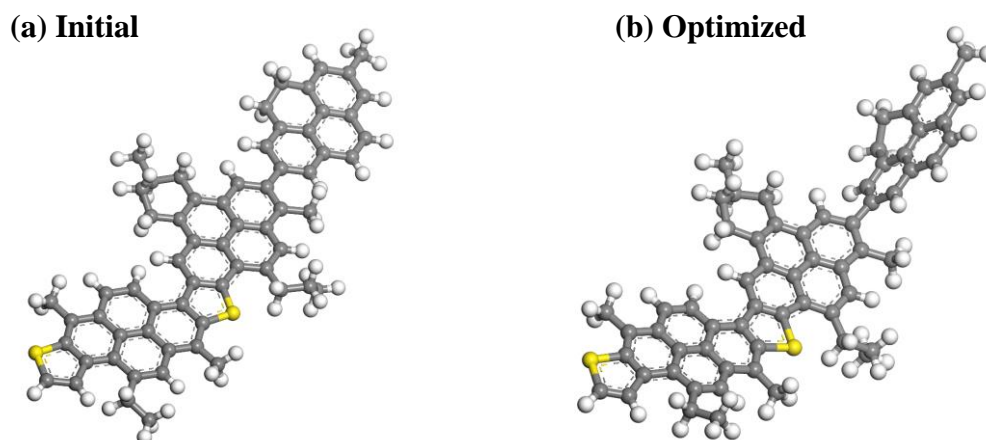


Figure 3.3. Example of structural changes in an asphaltene molecule before (a) and after (b) geometry optimization.

To assure that each of the molecules is placed in a reasonable conformation within the supercell (avoiding ring spearing or unreasonable contact between atoms) a preliminary supercell with a reduced density is constructed. In the case of this study such preliminary supercell was constructed with a density of 0.1 g/cm^3 . This value may seem completely unreasonable, but it decreases the chances of non-desired (and unreasonable)

contacts between molecules. Once this reduced density preliminary supercell is built, it becomes the starting system for a set of molecular dynamics simulations capable of shrinking the cell to the real correct density. For doing this, first a molecular dynamics simulation is conducted with the NVT ensemble, which keeps the volume of the cell constant while allowing the molecular structures to agglomerate under the action of the intermolecular forces driven by the force field. Second, a subsequent molecular dynamics simulation must be conducted with the NPT ensemble, which in addition to a thermostat, incorporates a barostat that equilibrates the volume of the cell (and therefore the density) according to a fixed value of external pressure (1 atm). Once this second molecular dynamics simulation reaches equilibrium, a reasonable final density value is obtained, which in the case of this study corresponds to 0.9 g/cm^3 . **Figure 3.4** illustrates the three states involved in the supercell construction process: **(a)** 0.1 g/cm^3 reduced

density, **(b)** agglomeration with NVT molecular dynamics, and **(c)** equilibration with NPT molecular dynamics reaching a density of 0.9 g/cm^3 .

After obtaining an asphalt supercell with a correct packing and density, supercells for the mineral phases need to be constructed as well. Unlike asphalt, which is an amorphous periodic system, the mineral phases are crystalline meaning that a lattice structure with a specific extended atomic array must be maintained in the simulation.

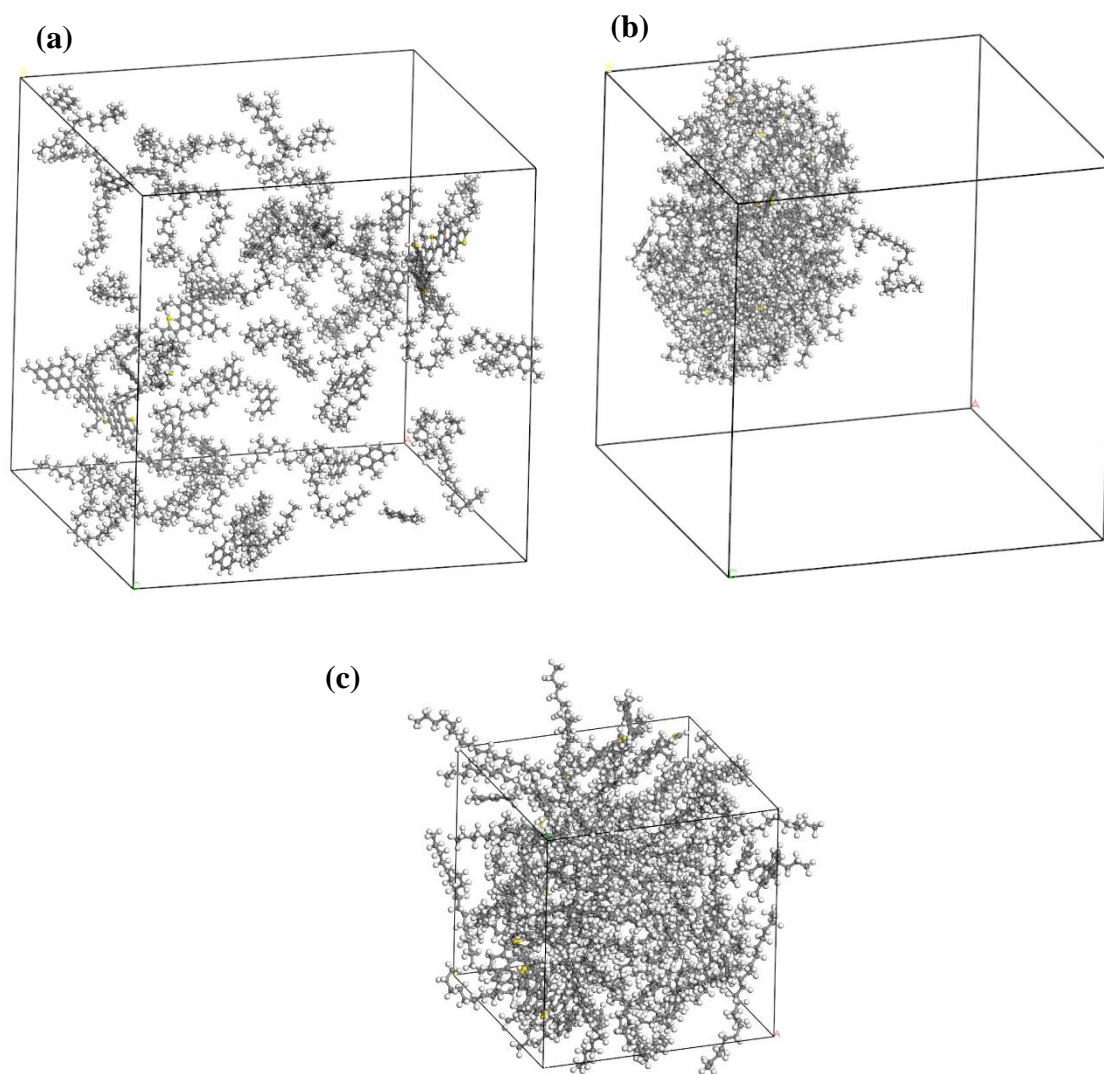


Figure 3.4. Construction process for the asphalt supercell: (a) cell with reduced density of 0.1 g/cm^3 , (b) agglomeration, (c) cell equilibrated to a density of 0.9 g/cm^3 .

Therefore, the geometry optimization of minerals must yield a periodic cell with dimensions and an atomic array almost the same as the experimental unit cell (which is usually the initial structure used as input). Other than this constraint, the optimization of mineral supercells is fairly straightforward, and if it is correct little or almost no change should be noticeable from the optimized cells.

The next step is to construct layered supercells that will contain the interface between the asphalt and the minerals. Such process involves a degree of complexity for the case of the minerals since cleavage along one plane of the supercell is required.

3.2.3.2.1. Construction of layered supercells

The construction of layered supercells is a step in which care must be taken as to properly cleave the correct plane of the mineral phases. After the correct cleavage planes are defined, it is possible to stack the asphalt and mineral phases together as if they were layers one on top of the other. Another important detail when constructing the layered supercells is that of the vacuum pad that must be included on top of the two phases to isolate the system from interacting with itself since the system is still periodic in all dimensions. Finally, of critical importance is the modification of the atom types and partial charges for the atoms at the surface of the minerals. If the partial charges are too high, the lattice array will be distorted to a great extent. **Figure 3.5** illustrates the constructed layered supercells for the systems in this study: (a) the asphalt-quartz interface, (b) the asphalt-calcite interface, (c) the asphalt-hydrated lime interface. **Figure 3.6** illustrates the distortion of the lattice array that occurs when having too high partial charges for the dangling atoms at the surface of the quartz crystal.

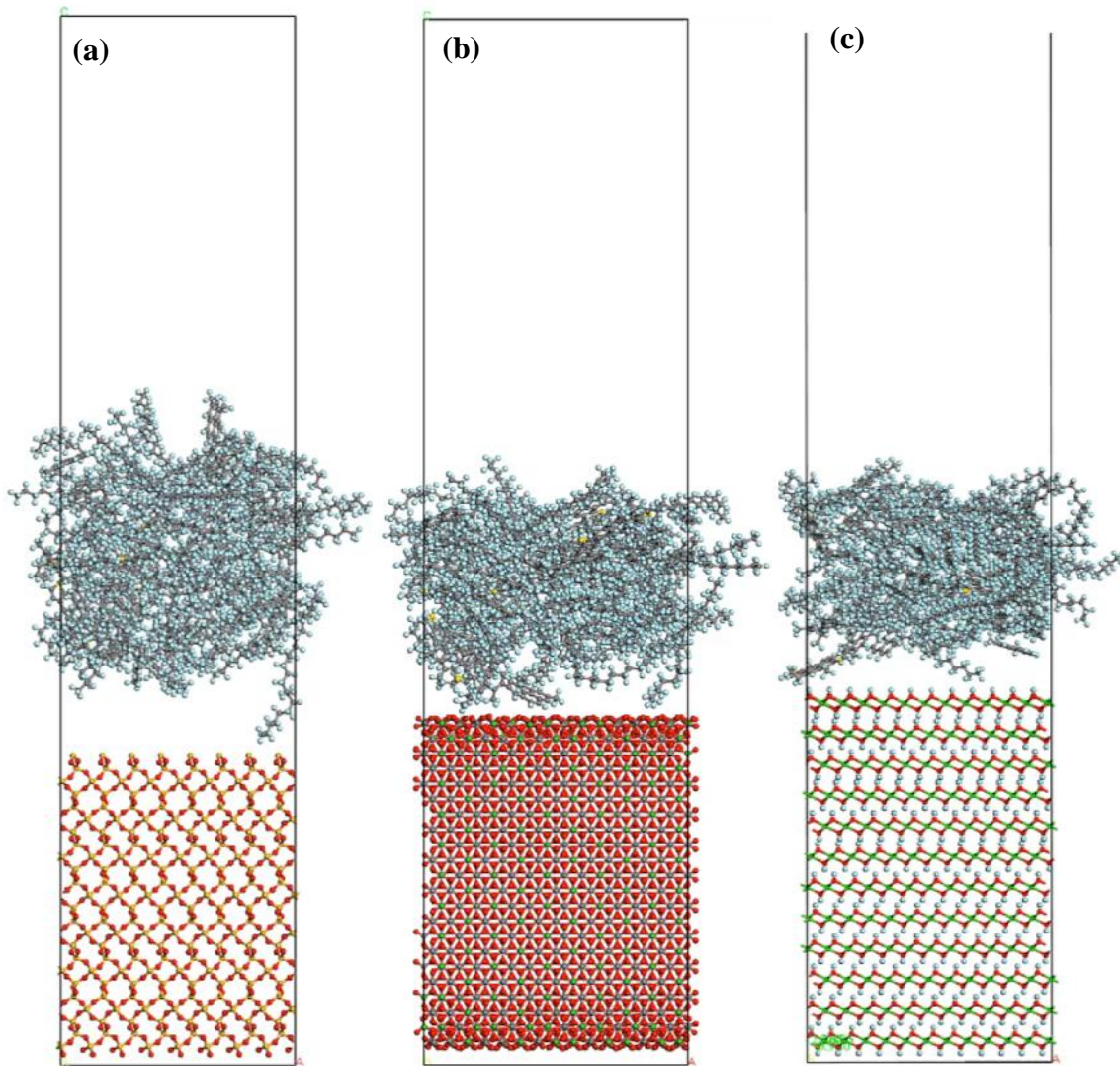


Figure 3.5. Layered supercells constructed: (a) asphalt-quartz, (b) asphalt-calcite, (c) asphalt-hydrated lime. Atom colors are dark yellow (Si), green (Ca), red (O), white (H), grey (C), and bright yellow (S).

After the construction of the layered supercells containing the interfaces between asphalt and the three minerals in study, and their adequate parametrization, the

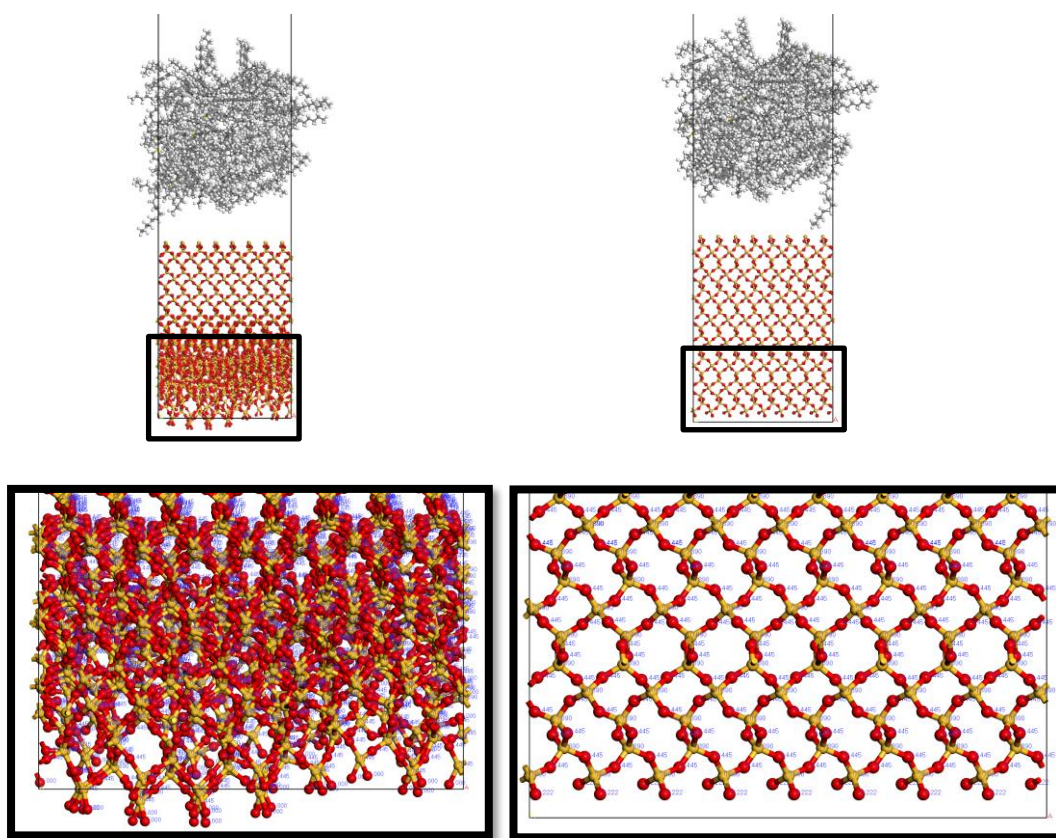


Figure 3.6. Effect of atom types and partial charges on dangling atoms at the cleaved surface of the quartz-asphalt interface.

energetics are calculated. This encompasses the calculation of the surface interaction energies, the estimation of the contact area, and the calculation of the work of adhesion, which is the end result of the classical simulation methodology proposed in this study. The detailed process along with explanations of each parameter are introduced in the next subsections.

3.2.3.3. Calculation of surface interaction energies

The surface interaction energies are potential energy values that correspond to the non-bonding interactions (electrostatic and van der Waals) generated at the surface

of a given phase due to the atoms with incomplete bonds as a result of the cleavage of the bulk phase. The first step in the methodology to obtain the surface interaction energies is to perform a molecular dynamics simulation with the NVT ensemble. This will allow the asphalt phase to change the conformation of its molecular species driven by the attractive or repulsive nature of the non-bonding forces exerted by the dangling atoms exposed at the mineral surface. Once the trajectory file is obtained after the molecular dynamics simulation has reached equilibration, a frame is extracted from the equilibrated region containing the geometry of the interacting interface. This frame is then used as the input structure for a single point energy (SPE) calculation to obtain the potential energy value of the interacting interface of the two phases, asphalt and mineral. Next, from this same frame, SPE calculations are also conducted for the asphalt phase and the mineral phase by separate. With these three values then, the surface interaction energy is obtained as the difference of the asphalt-mineral interfacial energy minus the energies of each phase by separate as follows in equation (22).

$$\Delta V_{interface} = V_{asphalt-mineral} - (V_{asphalt} + V_{mineral}) \quad (22)$$

A graphical depiction of each of the values in equation (22) is illustrated in **Figure 3.7**, where **(a)** is the interfacial system, **(b)** is the asphalt phase by separate, and **(c)** is the

mineral (quartz) phase by separate. Note that the three cases are obtained from a single frame.

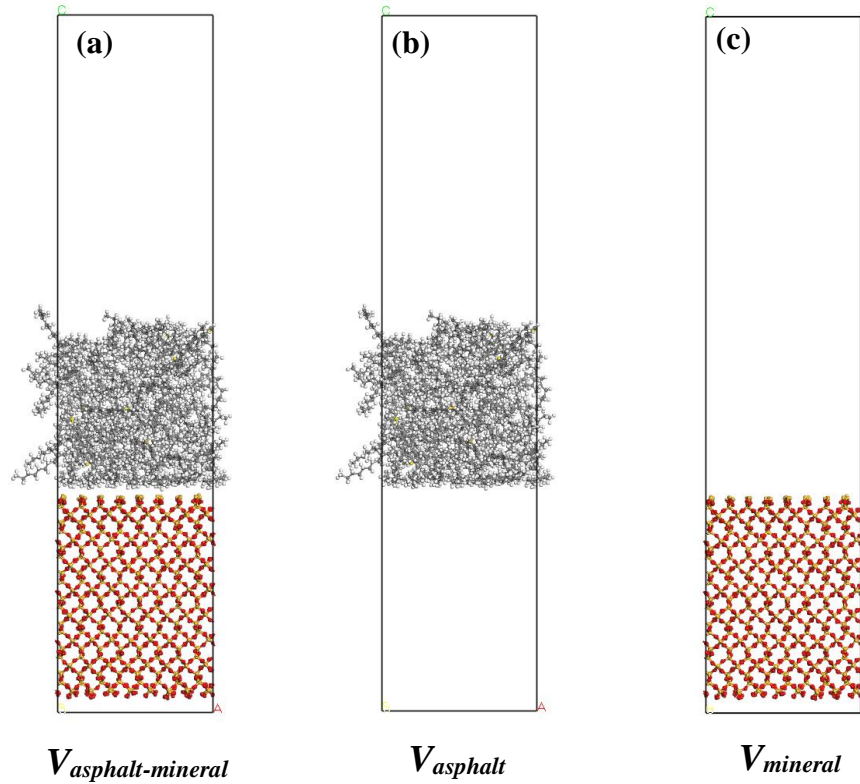


Figure 3.7. Graphical conceptualization of the interfacial energy components in equation (22).

3.2.3.4. Estimation of interfacial contact area

The contact area at the interface is required to calculate the work of adhesion between asphalt and mineral phases. Some degree of complexity accompanies the determination of this value since asphalt is an amorphous phase. Several options exist, some more simple than others. The simplest choice is to use the dimensional area (that of a flat cross-sectional plane having the dimensions of the layered supercell). However, a more refined methodology is proposed in this study. Within the capabilities of the

Materials Studio software suit, the area is calculated corresponding to the two-dimensional surface shaped by the van der Waals radii of the atoms exposed at the surfaces of each phase. This method is denominated Conolly surface fields and aids in accounting for the amorphous surface shape of the asphalt phase. However, an approximation is needed to combine the uniform surface of the mineral phase in conjunction with the amorphous surface of the asphalt phase. An average contact area is proposed in this study as follows in equation (23):

$$\text{Contact area} = \frac{1}{2} (A_{\text{asphalt}} + A_{\text{mineral}} - A_{\text{asphalt-mineral}}) \quad (23)$$

As an example, for the case of quartz, a graphical representation of each of the terms in equation (23) is illustrated in **Figure 3.8**: (a) composite system top and bottom, (b) asphalt phase top and bottom, (c) mineral phase top and bottom.

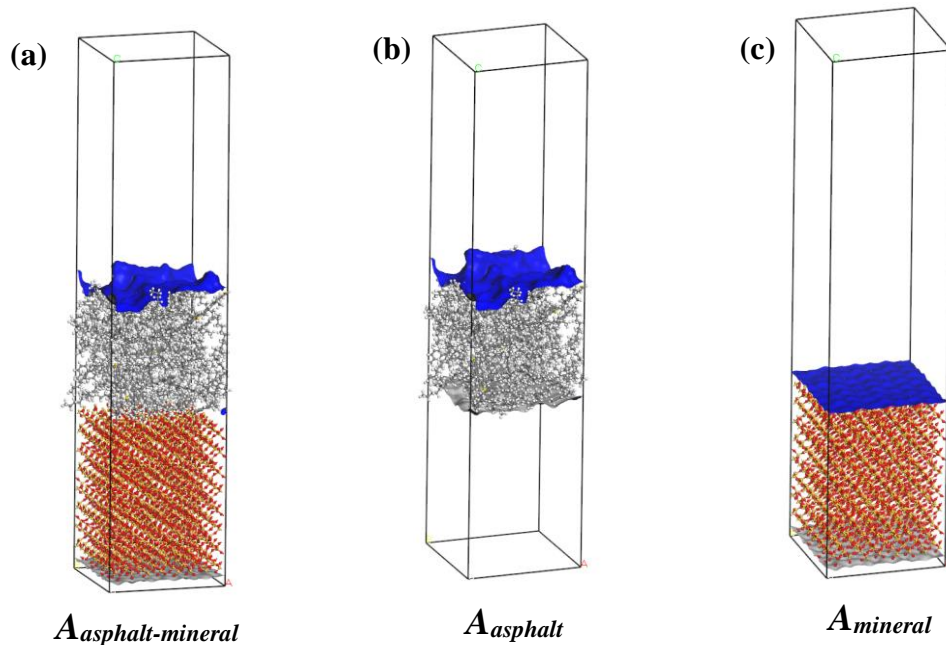


Figure 3.8. Conolly surface fields calculated for each system: (a) composite system, (b) asphalt only, (c) mineral only.

3.2.3.5. Calculation of the work of adhesion

With both the surface interaction energies and the contact areas determined, the work of adhesion of the interfacial system is computed. The work of adhesion is defined as the amount of external work required to separate two materials at their interface in a vacuum¹³. The value of computing the work of adhesion is that it represents an energetic measure of the strength of the non-bonding interactions between two phases normalized by the actual contact area upon which the adhesion forces are being exerted. The mathematical expression for obtaining the work of adhesion is defined in equation (24):

$$W_{adhesion} \left(\frac{kcal}{\text{\AA}^2} \right) = \frac{\Delta V (kcal / mol)}{A_{contact} \left(\frac{\text{\AA}^2}{molecule} \right) \times \left(\frac{6.022 \times 10^{23} molecules}{mol} \right)} \quad (24)$$
$$W_{adhesion} \left(\frac{erg}{cm^2} \right) = W_{adhesion} \left(\frac{kcal}{\text{\AA}^2} \right) \times \frac{4.184 \times 10^{10} erg}{kcal} \times \frac{\text{\AA}^2}{1 \times 10^{-16} cm^2}$$

3.2.4. Results and discussion

As the central aim of this work is the evaluation of the superiority of hydrated lime used in asphalt as an active filler in comparison to other fillers deemed as inert, the first step taken was to evaluate the non-bonding interactions of the three proposed fillers (hydrated lime, quartz, and calcite) with an asphalt model. As outlined in the previous section, the methodology proposed using classical mechanics simulation theory described in the theoretical background provides this exact information. The effects of physical factors induced by the model representation are further incorporated by computing not only the surface energies of interaction, but also the work of adhesion. As most of the calculation details have been thoroughly explained in the methodology

section, results are concisely summarized in the following tables and charts illustrated in

Figure 3.9.

$\Delta V_{asph-mineral} (kcal/mol)$		
Mineral	This study	Wang (2016) ¹⁴
Quartz	-161	-180
Lime	-262	---
Calcite	-454.5	-300

$W_{adhesion} (erg/cm^2)$		
Mineral	This study	Wang (2016) ¹⁴
Quartz	-89.4	-100
Lime	-107.3	---
Calcite	-170.23	-160

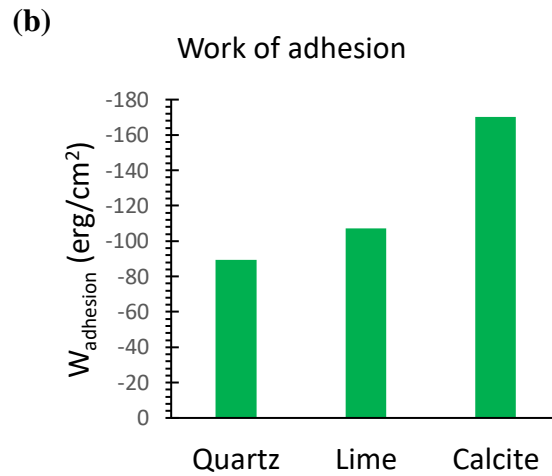
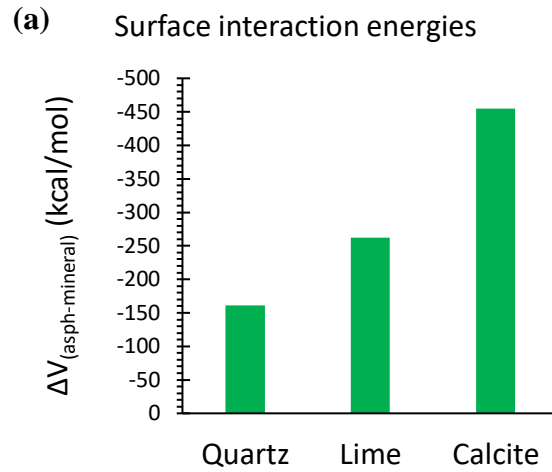


Figure 3.9. Summary of results obtained with classical molecular modeling: (a) interaction energies and (b) work of adhesion.

The clear tendency observed in these results is that hydrated lime does not exert superior non-bonding attraction forces on the asphalt model investigated. Rather than this, hydrated lime ranks in between the values of quartz and calcite. Such a ranking is not what would be expected. However, the values obtained in this study are supported by similar computational¹⁴ and experimental studies^{15,16}.

3.3. Quantum mechanics modeling

In an effort to overcome the limitations observed with the classical modeling approach, quantum calculations are implemented in this study to assess the reactivity of hydrated lime as a filler in asphalt. Due to the very high demand on valuable computer resources, simplified molecular systems are elaborated for both organic (asphalt) and mineral constituents. In the case of the mineral constituents, such simplification involves the consideration of discrete molecular units instead of extended periodic cells characteristic of crystalline systems. Similarly, for the case of asphalt a non-periodic system is considered instead of an amorphous periodic cell as it was the case in the classical molecular modeling approach. Even more, complex mixtures of large aliphatic or polycyclic aromatic hydrocarbon molecules are not attempted. Rather, specific small molecular species are implemented as surrogates of the macromolecular entities present in asphalt. These simplified molecular surrogates correspond to key components or major “building blocks” of asphalt macromolecular structures. The basis for this approach is that which Robertson¹⁷ proposed with the purpose of targeting the chemistry of asphalt in a direct and comprehensive way that could circumvent the complexities posed by the size and diversity of chemical entities present in asphalt. The following subsections introduce the molecular models used in this study.

3.3.1. Models of mineral fillers used in asphalt mixtures

As introduced in the previous paragraph, simplified systems have been devised to reduce the complexity of the quantum modeling approach. In the case of minerals the major simplification is the consideration of discrete molecular units instead of periodic

cells with extended atomic arrays characteristic of crystalline systems. Following this approach, this study seeks to mimic the bonding behavior of three specific minerals used as fillers in asphalt mixtures: hydrated lime (calcium hydroxide), quartz (silicon dioxide), and calcite (calcium carbonate). The surrogate models for mimicking the behavior of these three minerals are introduced in the following subsections.

3.3.1.1. Hydrated lime (calcium hydroxide)

To create a discrete molecular unit of hydrated lime, $\text{Ca}(\text{OH})_2$, it was first necessary to depart from the unit cell of hydrated lime as a crystalline system. As introduced in the classical molecular modeling section, the unit cell of hydrated lime is as shown in **Figure 3.10(a)**; where the calcium atoms are green, oxygen is red, and hydrogen is white. Once defined, the unit cell can be reduced as shown in **Figure 3.10(b)**. It is in this form that the discrete molecular unit of hydrated lime can be visualized and extracted as shown in **Figure 3.10(c)**.

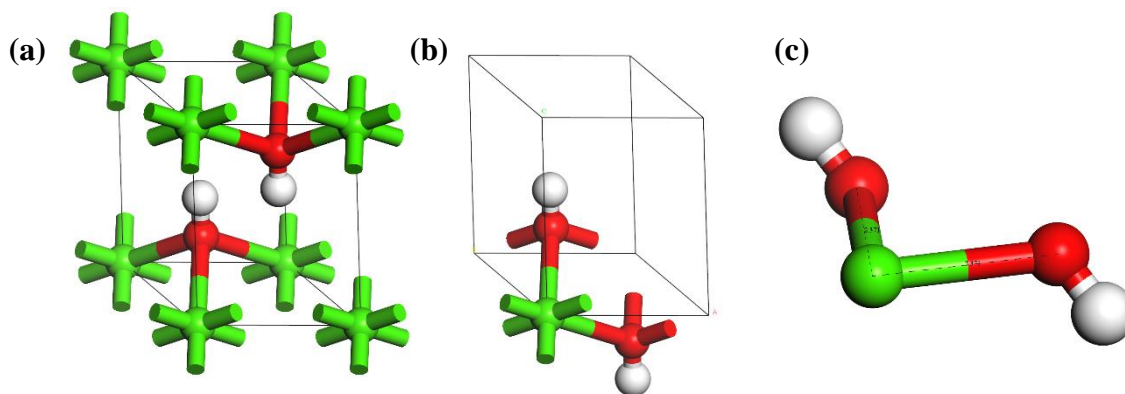


Figure 3.10. (a) hydrated lime unit cell, (b) reduced unit cell, and (c) hydrated lime discrete molecular unit. Atom colors are green (Ca), red (O), white (H).

3.3.1.2. Quartz (silicon dioxide)

Quartz is a tectosilicate therefore it is structured as a three-dimensional framework of silicon tetrahedra linked by oxygen atoms (SiO_4) that is often reduced to the chemical formula (SiO_2). Due to the stability of quartz as a mineral phase, it is less intuitive to single out a discrete molecular unit. However, taking as a basis the repeating tetrahedra that compose the three-dimensional framework, it is possible to conceive the idea of these as repeating units of a discrete molecular structure. Although in small concentrations, in aqueous solution such single building units do exist as orthosilicic acid (H_4SiO_4). Orthosilicic acid tends to polymerize readily to form larger structures that eventually reach crystallinity to form quartz. For this reason, in this study the surrogate chosen to mimic the behavior of quartz is pyrosilicic acid (the dimer of orthosilicic acid) as it is the smallest unit including a shared oxygen between two silica tetrahedra. **Figure 3.11(a)** illustrates the unit cell of a quartz crystal, and **Figure 3.11(b)** shows the molecular structure of pyrosilicic acid ($\text{Si}_2\text{O}_7\text{H}_6$).

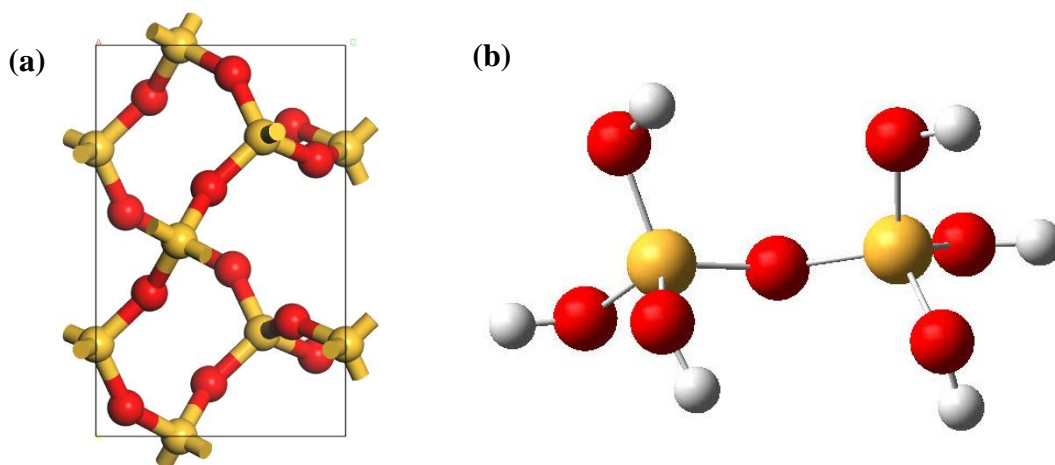


Figure 3.11. (a) Unit cell of a quartz crystal, (b) Structure of pyrosilicic acid, the molecular surrogate chosen to mimic the behavior of quartz. Atom colors are yellow (Si), red (O), white (H).

3.3.1.3. Calcite (calcium carbonate)

The crystalline structure of calcite is much more complex than that of hydrated lime or quartz. Several cleavage plains and ionic bonding environments can be identified between calcium atoms and carbonate anions in the lattice structure of the calcite unit cell. Furthermore, when thinking of ways to single out a discrete molecular unit representative of the calcite mineral, the geochemistry of the carbonate anion in aqueous media imposes a complex tri-phasic pH-dependent constraint. Based on the pK_a values of carbonic acid ($pK_{a1}=6.3$, $pK_{a2}=10.32$), the carbonate species that will predominate will be either carbonic acid ($pH < 6.3$), bicarbonate ($6.3 < pH < 10.32$) or carbonate ($pH > 10.32$). Because of these constraints, it is also necessary to consider what are the typical acid-base conditions of pure untreated asphalt ($6 < pH < 9$)¹⁸. For this reason, bicarbonate (HCO_3^{-1}) is chosen as the ligand for a calcium bicarbonate complex representative of calcite. **Figure 3.12(a)** illustrates the unit cell of calcite, and **Figure 3.12(b)** illustrates the simplified calcium bicarbonate complex.

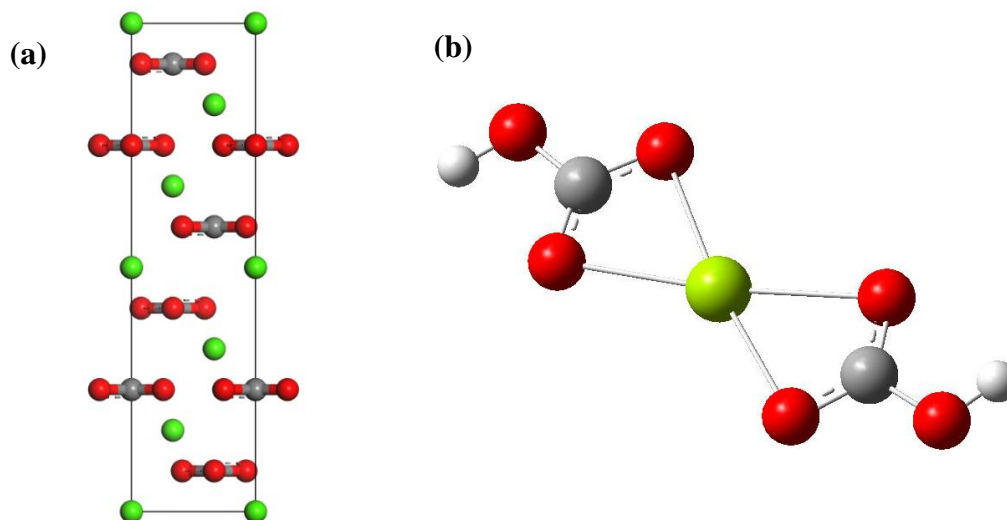


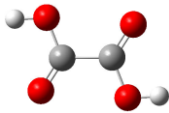
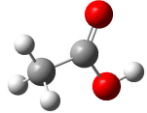
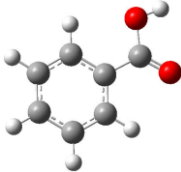
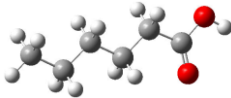

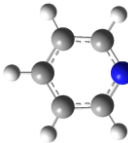
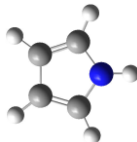
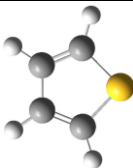
Figure 3.12. (a) Unit cell of calcite, (b) calcium bicarbonate complex surrogate for calcite. Atom colors are green (Ca), grey (C), white (H), and red (O).

3.3.2. Models of asphalt molecular building blocks

This computational study follows the molecular “building blocks” approach introduced from the work developed by Robertson¹⁷. This approach, according to Robertson, finds convenience in describing the composition of asphalt as an assembly or matrix of molecular species (the building blocks) that construct the large multi-molecular units within the asphalt. The rationale for this convenience is the ability to comprehensively evaluate and screen the diverse chemical interaction sites and the nature of such interactions.

Within the building blocks described by Robertson¹⁷, this study focuses on specific functional groups. These include in majority the evaluation of different carboxylic acids and heterocyclic structures including heteroatoms such as nitrogen and sulfur. **Table 3.2** provides a concise and illustrative list of the molecular species included in this study. As previously explained at the beginning of this chapter, the emphasis on the evaluation of several carboxylic acids is due to the problematic role that these species play in asphalt mixtures, one of the major reasons why lime is used as a filler. Some of the carboxylic acid species included in **Table 3.2** are not likely to be present in asphalt. This is the case of species such as oxalic acid and acetic acid. However, they were included in the study first due to their reduced number of atoms; and secondly, in the case of oxalic acid, due to the high reactivity of the species which can be utilized as a benchmark to evaluate the reactivity (or lack of it) of other carboxylic acid groups that are associated to larger hydrocarbon moieties.

Table 3.2. Molecular species investigated as surrogates of asphalt macromolecular moieties. Atom colors are red (O), grey (C), white (H), blue (N), and yellow (S).

Species	Formula	pKa	Model
Oxalic acid	$\text{H}_2\text{C}_2\text{O}_4$	1.25, 4.14	
Acetic acid	CH_3COOH	4.756	
Benzoic acid	$\text{C}_6\text{H}_5\text{COOH}$	4.202	
Hexanoic acid	$\text{C}_5\text{H}_{11}\text{COOH}$	4.88	
Dodecanoic acid	$\text{C}_{11}\text{H}_{23}\text{COOH}$	5.3	
Pyridine	$\text{C}_5\text{H}_5\text{N}$	5.25	
Pyrrole	$\text{C}_4\text{H}_4\text{NH}$	17.5	
Thiophene	$\text{C}_4\text{H}_4\text{S}$	---	

3.3.3. Modeling methodology and parameters of interest

Having defined the molecular models to be investigated, the computational details and methodology proposed to obtain the desired parameters that will help

corroborate the experimental data supporting the reactive nature of the interactions between hydrated lime and asphalt can be introduced. This methodology also seeks prediction of comparative values and trends for the interactions between the other two proposed fillers: quartz, and calcite; and furthermore, qualitative and quantitative inferences on the chemical reaction mechanisms explaining such interactions. To do this, there are two major parameters or indicators that this study seeks: the strength of the bonds formed when a mineral filler complexes with carboxylic acids and other proposed organic moieties, and the character of the bonding developed in these complexes. Furthermore, a key environmental constraint investigated is the effect of pH on the composition and reactivity of the species in study, and its impact on the strength and nature of the organo-mineral complexes.

3.3.3.1. General computational details

The level of theory used in this segment of the study is density functional theory (DFT). As introduced in the theoretical background section, the goal of this theoretical approach is to find the total energy of the atomistic system as a functional of the electron density function $\rho(\mathbf{r})$. In the following subsections, each of the key computational details that are general over all the calculations will be specified and briefly described.

3.3.3.1.1. Functional for the calculations

Upon an initial set of calibration trials with the hydrated lime molecule, convergence criteria were met faster with the PBE (Perdew-Burke-Ernzerhof) functional^{19, 20}. The B3LYP (Becke, 3-parameter, Lee–Yang–Parr)²¹⁻²³ functional was also tested and convergence was not as fast and complete as with the PBE functional.

3.3.3.1.2. Basis set

Because the models were simplified to be discrete molecular systems instead of periodic systems, the use of plane waves (spatially extended functions) to define the basis functions was not necessary. Instead, gaussian functions (spatially localized functions) define the basis functions used in the basis set expression. Following this criterion, the Pople ²⁴ basis set with polarization and diffuse functions 6-311⁺⁺G(3d,3p) was chosen to optimize convergence.

3.3.3.1.3. Implicit solvation model

Another subsequent condition defined based upon the discrete molecular system definition is the usage of an implicit solvation model. The picture to have in mind when an implicit solvation model used is that the discrete molecular structures are surrounded by or isolated in an infinite continuum representing the selected solvent in which the calculation is desired. In this study, the SMD ²⁵ solvation model was used to define a solvation cavity for the species that were defined explicitly, which incorporates the solvation energy component into the calculation of the total energy of the system. In all cases, two solvents were simulated. First, **water** as to capture and represent the behavior of the species or complexes surrounded by an extreme benchmark condition of a water continuum; and secondly, since the pure medium in which these complexes are to form is asphalt, **n-dodecane** was chosen as an aliphatic non-polar matrix representative of the paraffinic dispersant solvent-like phase (oils) of an asphalt mixture.

3.3.3.2. Determination of the bonding strength

Materials engineers are always searching for better ways of determining the strength of a material or composite. Experimentally, a vast set of methods exist at the macroscale, microscale, and even nanoscale. Modeling-wise the most common (and usually feasible) way is through the usage of continuum models. However, when dealing with chemical phenomena all these methods tend to fall short in providing direct causative explanation of the strength gain mechanism. For this reason, this study seeks to develop an atomistic modeling methodology to define the strength of a bond formed between two or more atoms of different molecular species explicitly defined in a physical system. A very useful and common way in which the strength of chemical bonds are quantified in chemistry fields is energetically: in terms of kilocalories per mol (kcal/mol). The key concept in this study is the bond dissociation energy (BDE), defined for atoms of a same molecule (intramolecular bonds) when they undergo reactions that involve the breakage of such bonds²⁶. A similar concept could be imagined then for atoms of different molecules in complexation. That concept can be brought to reality when having the capability of calculating the total energy of an atomistic system, just as DFT theory allows. Through the application of DFT theory and algorithms, and the implementation of a modeling suite (Gaussian 16)^{27, 28} capable of performing energy calculations, this study has found a prediction methodology for energetically verifying the stability and strength of a given molecular system in complexation. In this case, the system of interest is the complexation between the hydrated lime and asphalt moieties defined in sections 3.3.1 and 3.3.2.

3.3.3.2.1. Calculation of dissociation energies

The final result of an energy calculation in Gaussian 16 (in this case geometry optimization and frequency calculation) is a set of thermochemical parameters under a section denominated “Thermochemistry” provided by the accompanying graphical interface software GaussView 6. Within those, the parameter of interest is the total energy of the system, “Sum of electronic and thermal free energies”. This means that both the electronic and thermal components of the free energies of reaction (G) are obtained. With this value, it is possible to determine whether dissociation is favored or not depending on the sign of ΔG ; as well, a quantitative inference can be made for the strength of the interaction depending on the numeric value of ΔG given in units of kcal/mol. In the case of this study, since the idea is to model dissociation, a positive value of ΔG means that the complex is stable, whereas a negative value of ΔG indicates that dissociation is favored under the environmental conditions of a chosen solvent. The dissociation energy is calculated then according to equation (22), as the difference between the free energies of the complex (AB) and that of the isolated dissociated components A and B (non-interacting) in a given solvent:

$$\Delta G_{dissociation} = G_{complex\ AB} - (G_A + G_B) \quad (25)$$

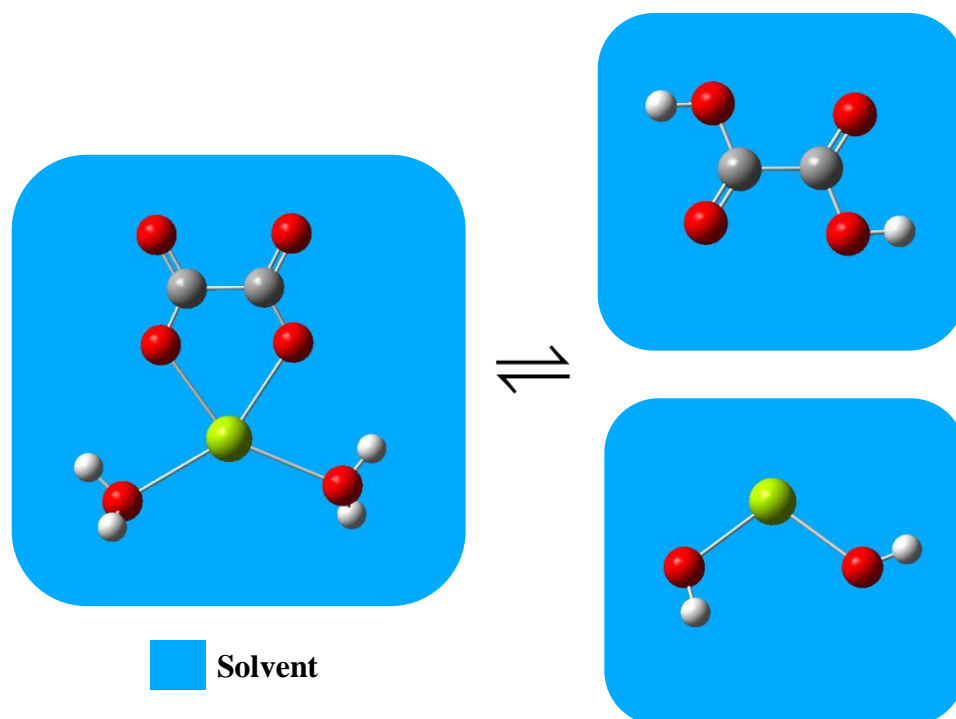


Figure 3.13. Graphical depiction of a dissociation reaction: calcium oxalate dissociating into oxalic acid and hydrated lime. Atom colors are green (Ca), red (O), grey (C), and white (H).

The graphical depiction of this reaction scenario is shown in **Figure 3.13**, where a calcium oxalate complex dissociates into oxalic acid and hydrated lime. On the left side of the scheme the complex and its energy are obtained, whereas on the right side the energies of the isolated species are obtained as if they were completely non-interacting.

Following this conceptual approach, the energies of dissociation of the models specified in sections 3.3.1 and 3.3.2 were determined in both water and n-dodecane. In addition, the energy of dissociation of the organic moieties representative of asphalt was determined for the case of an isolated calcium ion Ca^{2+} , mimicking the case in which hydrated lime is able to release free calcium ions into each of the two solvents specified above. In a systematic way, a testing matrix could be constructed which allows several

tendencies to be detected. This matrix is presented in section 3.3.4.1 along with the obtained results.

3.3.3.3. Determination of the bonding character

The Laplacian of the electron density is used to assess the ionic or covalent character of the complexes in study. With the aid of the software GausView 6, it is possible to generate slices along the bonds between atoms containing contour plots of isolines of the Laplacian of the electron density, which indicate the regions in which the change in the gradient of the electron density rises (negative values) or where it depletes (positive values).

3.3.3.4. Evaluation of the impact of pH

Almost all chemical species will exhibit transformations in structure and reactivity caused by the pH of the surrounding solvent. A relevant example previously discussed is that of the speciation of carbonate species (see section **3.3.1.3**) for the mimicking of the calcite mineral. As well, the organic species proposed as building blocks of asphalt exhibit variations defined by their pK_a values, which are specified in **Table 3.2**. Despite that the typical pH range for pure untreated asphalt is $6 < \text{pH} < 9$, for matters of simplicity a starting point chosen to develop the matrix of results for dissociation energies defined previously in section **3.3.3.2.1** was an extremely acidic (pH < 1.25) condition. The reason for this is that benchmark species investigated such as oxalate will remain protonated under such pH conditions as depicted on the right side of the reaction scheme shown in **Figure 3.13**, which makes easier the modeling performance as no charged species are to be explicitly specified. This analysis was

conducted for the case of hydrated lime and quartz only, and it is valid for cases of asphalt modified with polymers that can reach acidic values ($\text{pH} < 3$) that are below the pK_a threshold of weaker carboxylic acid species in study such as acetic acid, benzoic acid, hexanoic acid, and dodecanoic acid. However, when attempting to define the reaction system for calcite, a more refined analysis is needed due to the pH dependency of the carbonate anion present in the mineral as discussed in section **3.3.1.3**. This involves the assumption of a pH value within the typical range specified for pure untreated asphalt ($6 < \text{pH} < 9$) under which specific speciation occurs and charged species are then explicitly defined. This analysis was conducted for the two minerals that could have the potential to react (hydrated lime and calcite), but only in complexation with the benchmark species oxalate.

To better understand the rationale of the analysis, the graphical depiction of the reaction scheme for hydrated lime in **Figure 3.14** is examined to describe the reaction in terms of complex formation rather than dissociation. On the right side of **Figure 3.14**, a lime molecule is added as a slurry ($\text{pH} = 12.45$), and by assuming an initial $\text{pH} = 6.5$ condition for the asphalt phase with water as the solvent, oxalic acid will predominate as dissociated oxalate ($\text{C}_2\text{O}_4^{2-}$) and two hydroniums (H_3O^+). The two hydroniums will protonate the newly available hydroxyl ions of the hydrated lime molecule yielding two new water molecules. Subsequently, this allows the complexation of the calcium ion with oxalate as the ligand. As well, the two newly formed water molecules will coordinate with the Ca-oxalate complex along with the water molecules that previously conformed the hydroniums.

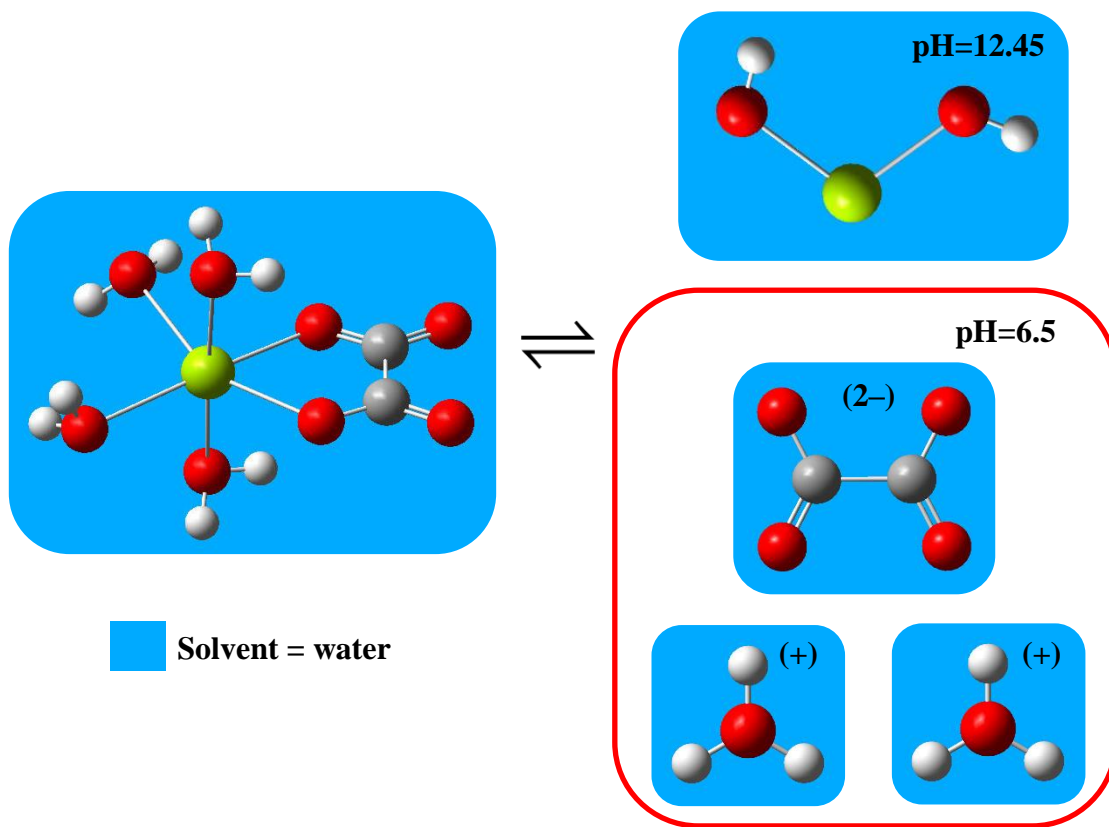


Figure 3.14. Graphical scheme of the reaction when a hydrated lime molecule (pH=12.45) is the mineral filler introduced in an aqueous system with pH=6.5, value at which oxalic acid has dissociated into the charged species oxalate and two hydroniums. Atom colors are green (Ca), red (O), grey (C), and white (H).

In this way, a calcium oxalate tetrahydrate complex $\text{CaC}_2\text{O}_4 \cdot (4\text{H}_2\text{O})$ will form (left side of **Figure 3.14**). The question tested by the modeling approach is then: will the calcium oxalate tetrahydrate complex have the thermochemical potential to form? The reverse question also applies: will the calcium oxalate tetrahydrate complex dissociate into the specified initial individual species? The answer is obtained by computing the same energetics as outlined in section **3.3.3.2.1**.

The calcite model system also needs brief mention as there is a slight difference from the hydrated lime model system. The reaction scheme for the calcite model is illustrated in **Figure 3.15**. In this case, the difference is that the hydroniums released by the oxalic acid are only able to hydrogen bond with the bicarbonate anions present in the calcite model. Thus, the calcium complex formed contains both anions: oxalate and bicarbonate.

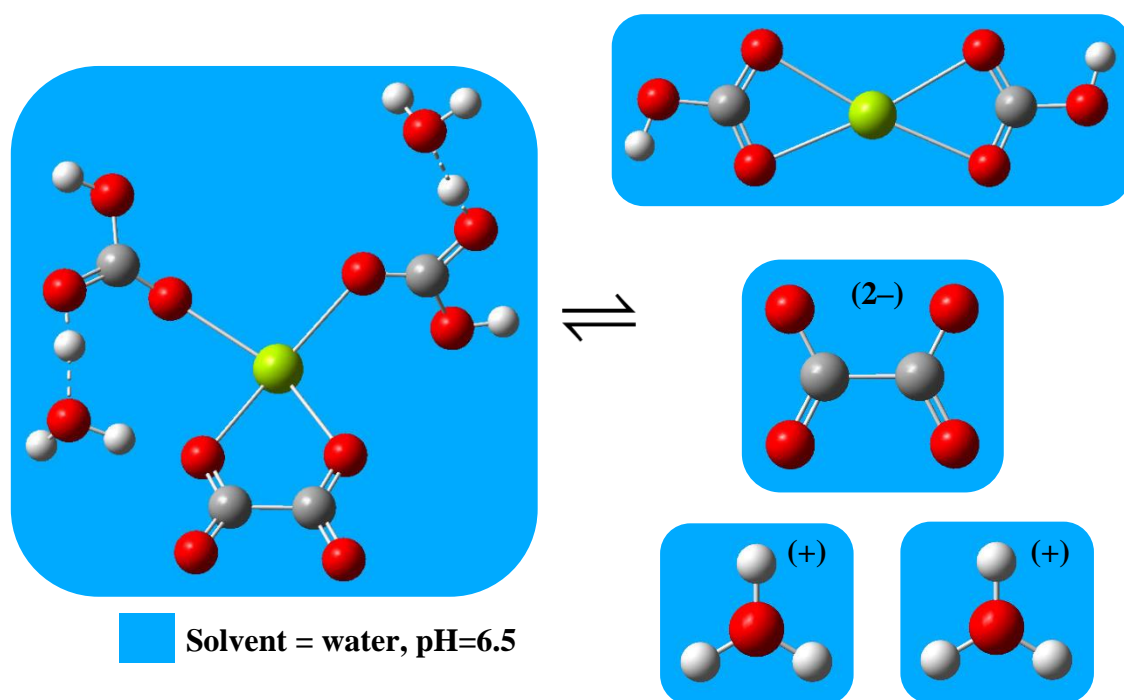


Figure 3.15. Graphical scheme of the reaction when calcium bicarbonate (model for calcite) is the mineral filler introduced in an aqueous system with pH=6.5, value at which oxalic acid has dissociated into the charged species oxalate and two hydroniums. Atom colors are green (Ca), red (O), grey (C), and white (H).

3.3.4. Results and discussion

3.3.4.1. Dissociation energies for benchmark pH < 1.25

As specified in section 3.3.3.4 simulations were conducted initially for the asphalt models defined in section 3.3.2 with the models of hydrated lime and quartz only, and the addition of the case of an isolated calcium ion Ca^{2+} . The matrix of cases that were simulated are shown next in **Table 3.3**, where the resulting value of dissociation energy is indicated for each case. These values of dissociation energy correspond to the benchmark condition of acidity (pH < 1.25) for the asphalt phase according to the reasons already explained in section 3.3.3.4.

In **Table 3.3** for the most part dissociation energies have a positive sign for carboxylic acid moieties (cells in green), meaning that these complexes are stable in both solvents simulated. In the case of the heterocyclic moieties the values of dissociation energies are for the most part negative (cells in red), meaning that these complexes are not stable, and dissociation is favored.

The second major trend gathered from **Table 3.3** is that of the difference in the outcomes for the dissociation energy values when varying the solvent (water vs. n-dodecane). Dissociation energies tend to be higher for all the minerals investigated (along with the case of isolated Ca^{2+}) when n-dodecane is the solvent. This trend can be visualized next in the bar charts shown in **Figure 3.16** and **Figure 3.17**.

Table 3.3. Matrix with dissociation energy values obtained for hydrated lime, Ca²⁺, and quartz models.

Dissociation energies, kcal/mol						
	Ca(OH)₂		Ca²⁺		Si₂O₇H₆	
	water	n-dodecane	water	n-dodecane	water	n-dodecane
ox	36.99	26.06	12.93	247.87	4.76	38.81
ac	23.73	41.93	5.95*	237.39*	2.54*	21.48
bz	25.73	43.13	4.48		2.40	20.78*
hex	20.86	39.23	5.19	238.62	2.39	19.34
doc	19.91	37.92	3.63	240.11	1.08	21.32
pydn	-9.80	4.15	-6.62	11.30	-5.00	-0.59
thio	-9.51	-4.82	-6.19	19.56*	-8.43	
pyol	-9.75	0.71	-5.78	29.19	-4.74	-5.23

ox = oxalate, **ac** = acetate, **bz** = benzoate, **hex** = hexanoate, **doc** = dodecanoate,

pydn = pyridine, **thio** = thiophene, **pyol** = pyrrole

*imaginary mode found

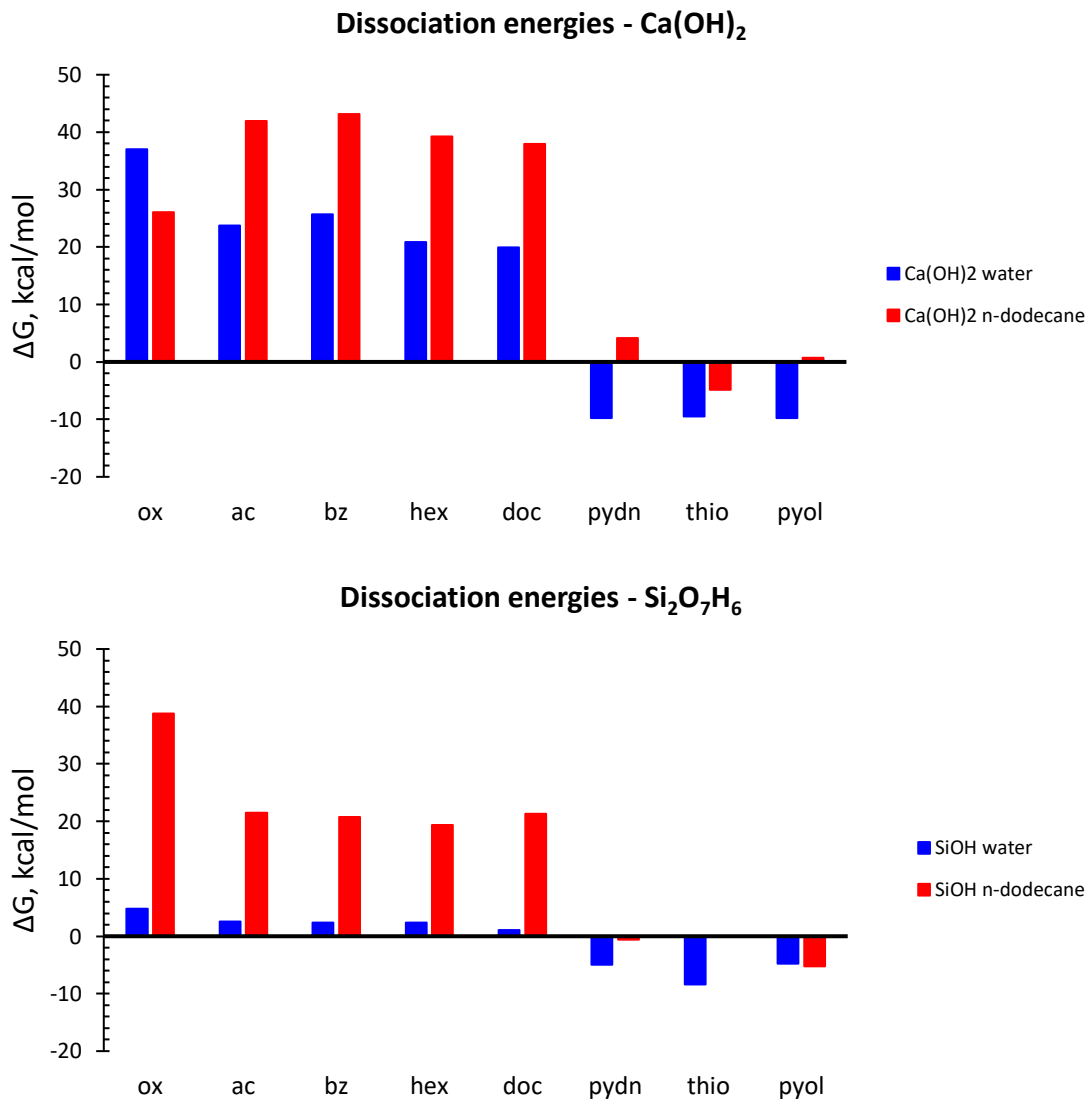


Figure 3.16. Comparison between dissociation energies in water vs. n-dodecane for hydrated lime and pyrosilicic acid.

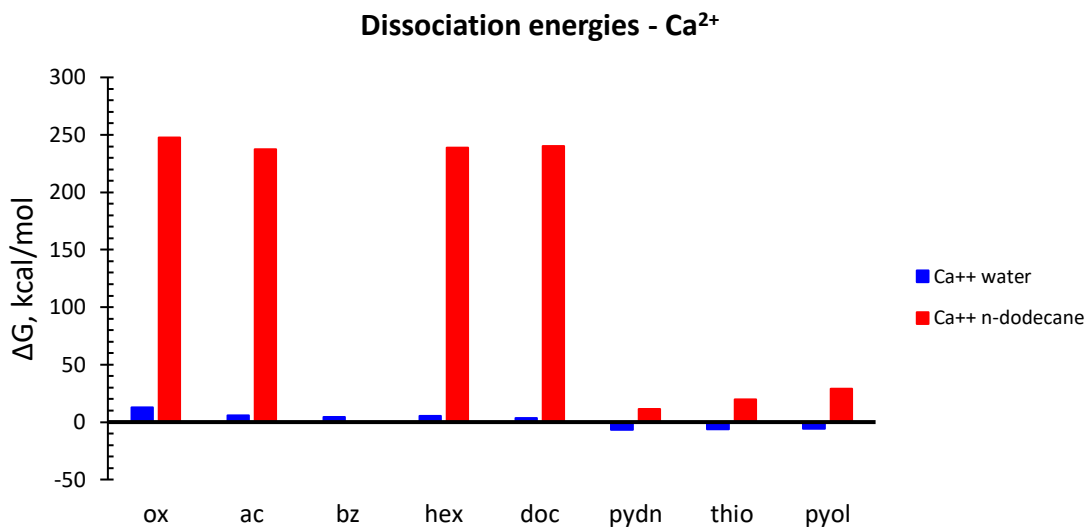


Figure 3.17. Comparison between dissociation energies in water vs. n-dodecane for an isolated Ca²⁺ ion.

The third important trend to remark from **Table 3.3** is that between the dissociation energy values of carboxylic acid complexes with hydrated lime versus quartz in water as the solvent. The bar chart shown in **Figure 3.18** illustrates the comparison in which complexes formed in presence of hydrated lime are substantially stronger.

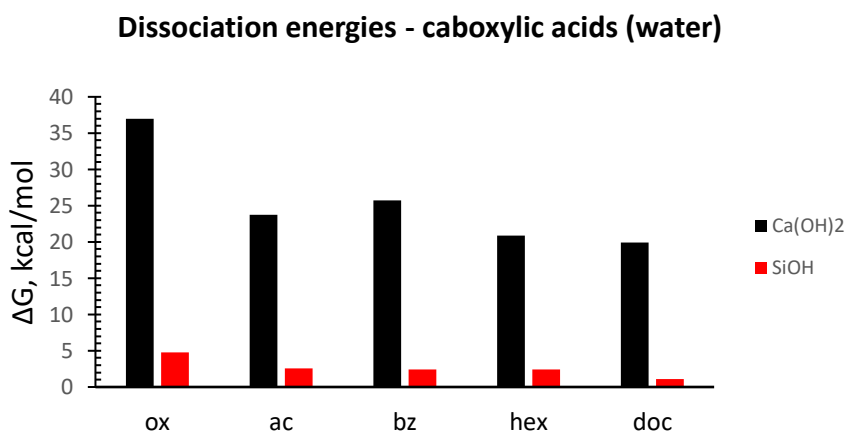


Figure 3.18. Dissociation energies of carboxylic acid complexes in presence of hydrated lime versus quartz in water as the solvent.

The fourth trend to remark from **Table 3.3** is that of the behavior of heterocyclic moieties, which only show positive values of dissociation energy for the case of an isolated Ca^{2+} ion and hydrated lime with n-dodecane (**Figure 3.19**).

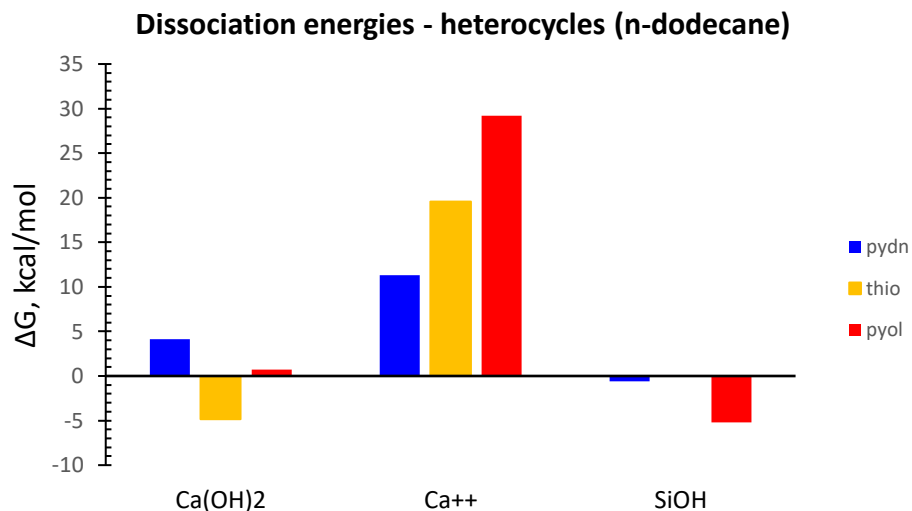


Figure 3.19. Dissociation energies of heterocyclic moieties in n-dodecane as the solvent. (pydn = pyridine, thio = thiophene, pyol = pyrrole)

3.3.4.2. Dissociation energies for a pH = 6.5 condition

Following the refined analysis outlined in section 3.3.3.4, a single simulation case with oxalate in water was conducted for the two mineral filler models with potential reactivity: hydrated lime and calcite. These two are shown in **Figure 3.20**, along with the value obtained for pyrosilicic acid for comparison. The difference between the dissociation energy of hydrated lime and that of the calcite model is significant, indicating that hydrated lime provides a superior bonding strength. As well, the value for

the dissociation energy of hydrated lime shows a substantial increase as compared with the simplified analysis results in **Table 3.3**.

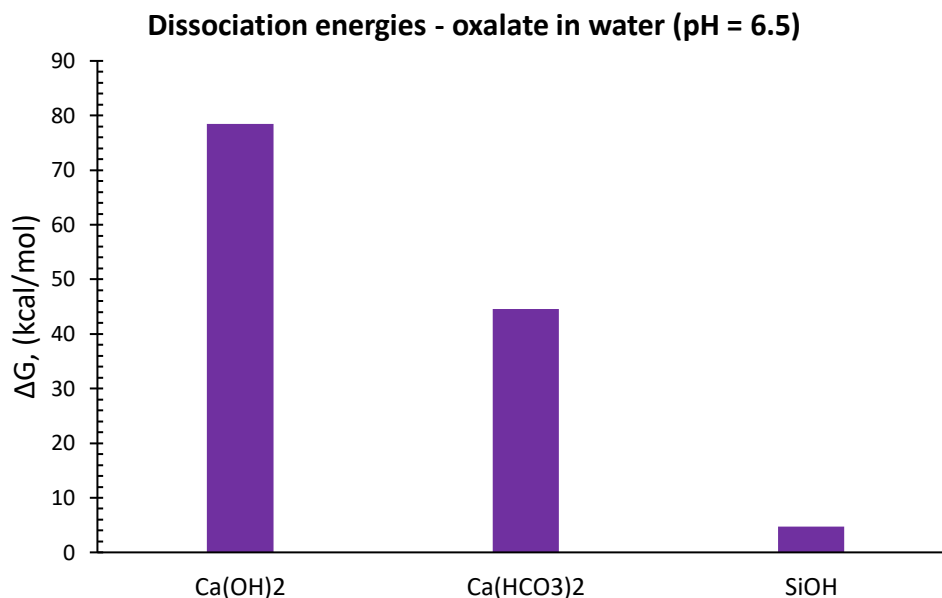


Figure 3.20. Dissociation energies for hydrated lime, calcite, and quartz models (pH = 6.5).

3.3.4.3. Results for the bonding character

The bonding character was qualitatively assessed as indicated in the methodology section with slices along the bonds between atoms containing contour isolines of the Laplacian of the electron density. **Figure 3.21** shows such contour map for the calcium oxalate complex. It is appreciable how the isolines with negative values for the Laplacian (purple) are continuous throughout covalent bonds such as that between carbon and oxygen (C-O) and carbon-carbon (C-C). In contrast, the bonds between calcium and oxygen (Ca-O) show a discontinuity with depletion of electron density along the along the bond (brown isolines), meaning that the bonds are of an ionic

character where electrons are not being shared across the two atoms. As a comparison, the bonds between sodium (Na) and chloride (Cl) are shown in **Figure 3.22** which is a typical example of an ionic bond.

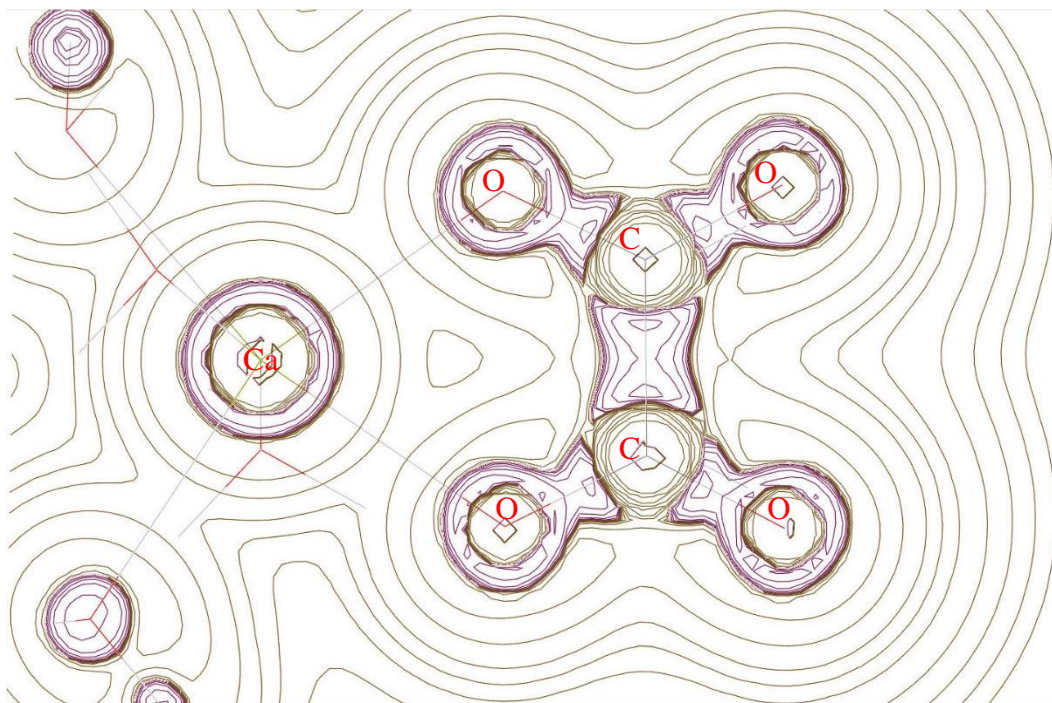


Figure 3.21. Contour map of the Laplacian of the electron density for the calcium oxalate complex.

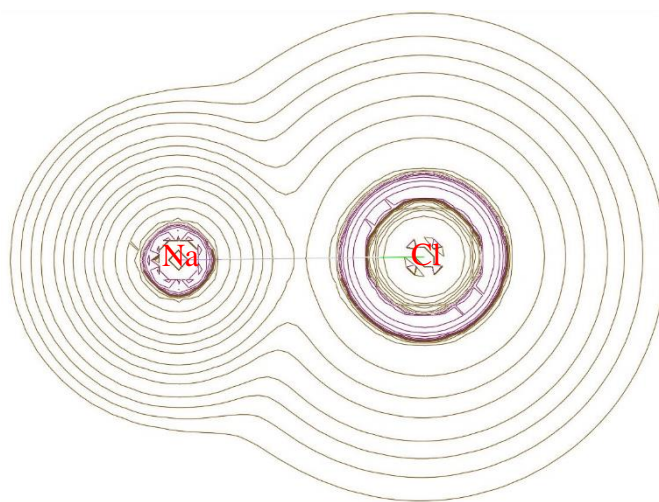


Figure 3.22. Example of the contour map of the Laplacian of the electron density for a typical ionic bonding case between sodium and chloride.

3.3.5. Agreement with experimental data

One of the principal goals of this quantum modeling study was the validation of existing experimental data supporting the reactive nature of hydrated lime when used as a mineral filler in asphalt. Specifically, this modeling study aimed at validating the data by Petersen ⁷, indicating a selectivity of hydrated lime for reaction with carboxylic acids present in asphalt. The modeling results presented in the quantum modeling section show agreement with the experimental data by Petersen, specifically the adsorption data shown in **Table 3.4**, which specifies the concentrations in mol/L of strongly adsorbed functional groups for both high calcium lime and dolomitic lime, and in which a major trend is appreciable favoring the adsorption of almost only carboxylic acid groups present in the asphalt mixtures investigated.

Table 3.4. Experimental data from Petersen validating the reactive nature of hydrated lime with asphalt ⁶.

	High calcium lime		Dolomitic lime	
	Strongly adsorbed	Not adsorbed	Strongly adsorbed	Not adsorbed
Percent of total asphalt (%)	5.64	94.36	4.73	95.27
Functional groups, mol/L				
Ketones	0	0	0	0.03
Anhydrides	0	0	0	0
Carboxylic acids	0.83	0.003	0.80	0.005
2-Quinolone	0.15	0.014	0.23	0.013
Sulfoxides	0	0.03	0	0.03

4. INTERACTIONS BETWEEN A TERPOLYMER AND SOIL MINERALS

In this segment of the study an investigation is presented on the chemical stabilization of soil minerals with a novel polymer formulation called a terpolymer. A terpolymer is a tri-block co-polymer in which the repeating unit is composed of three structures with functional groups of different charge character: anionic, cationic, and non-ionic. The terpolymer candidate investigated is in essence an acrylamide-based chain modified to yield the aforementioned variations in charge character for each repeating unit. For this reason, the acronym TPAM was the final denomination assigned, which stands for “ter-polyacrylamide”. By having all the possible sites (polar-neutral, positive, and negative), the terpolymer would be capable of developing strong interactions with the majority of the various minerals present in soils.

The scope of the investigation is limited to the understanding and explanation of the experimental methods utilized in the synthesis and validation of the structure and composition of the terpolymer TPAM, and insights of the terpolymer structure and behavior obtained through atomistic modeling techniques.

4.1. Experimental synthesis procedure

The synthesis procedure was a variant of the atom transfer radical polymerization technique (ATRP) as proposed by Patrizi ²⁹. The procedure is summarized in two major stages: the synthesis of the cationic co-polymer, and the subsequent hydrolysis of the cationic co-polymer in basic media with sodium hydroxide (NaOH), which yields a

percent of anionic moduli. The final product is then a terpolymer chain composed of repeating units each with three moduli (m, p, q).

The TPAM repeating unit consists then of a non-ionic polar acrylamide module (m), an anionic sodium acrylate module (p), and a cationic (3-Acrylamidopropyl)-trimethylammonium chloride (AMTAC) module (q). Such structure and composition is achieved following the two-stage procedure already stated above.

4.1.1. Synthesis of the cationic co-polymer (stage 1)

The terpolymer TPAM is an acrylamide-based chain. Therefore, the prime component to start the synthesis was the acrylamide monomer. To begin, the acrylamide monomer (AM) powder is mixed with the cationic monomer AMTAC in a polymerization promoter solvent, in this case N,N-dimethyl formamide (DMF) and a fraction of distilled water. Next, cuprous chloride and Tris(2-aminoethyl)amine (TREN) are mixed in a Schlenk tube to create a complex that along with an initiator methyl-2-chloropropionate (MCP) is added to the initial AM/AMTAC mixture to yield the AM:AMTAC cationic copolymer, which is finally precipitated with excess acetone and

dried in an oven at 40°C. **Figure 4.1** illustrates the setup used for this stage, and the appearance of the intermediate co-polymer product.

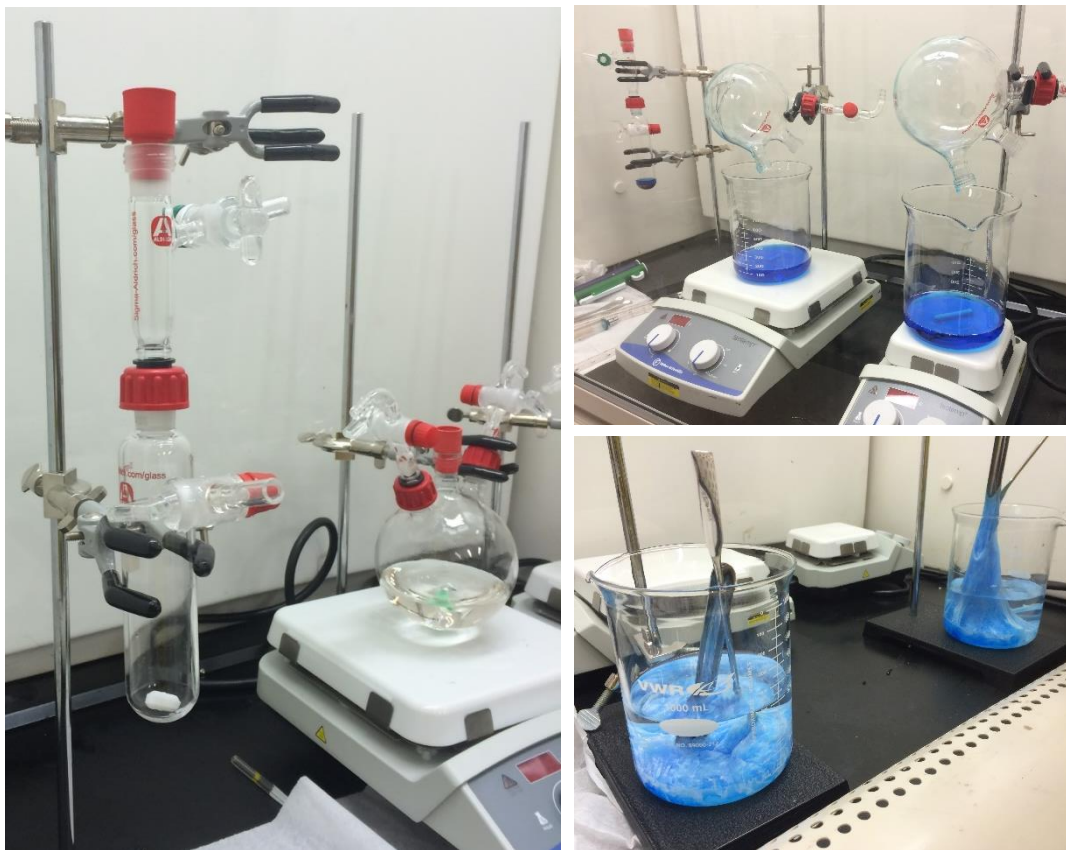


Figure 4.1. Synthesis of the cationic co-polymer AM:AMTAC.

4.1.2. Synthesis of the terpolymer via hydrolysis (stage 2)

In this second stage the dried product of stage 1, the cationic co-polymer AM:AMTAC, is hydrolyzed to convert a fraction of the acrylamide units in the chains into acrylate units. To do this, a sodium hydroxide solution is prepared with a 3M concentration, and placed in a round bottom flask. Then, an amount of the solid AM:AMTAC cationic co-polymer is added to the NaOH solution. The round-bottom

flask is then connected to a condenser, and the system is allowed to react for 12 hours. After these 12 hours, the liquid product is precipitated in excess methanol to obtain the terpolymer TPAM, which has white color and the consistency and appearance of “cotton candy”. The TPAM precipitate is dried at 40°C and a glue-like solid is obtained as the final product. **Figure 4.2** illustrates the setup and final product.

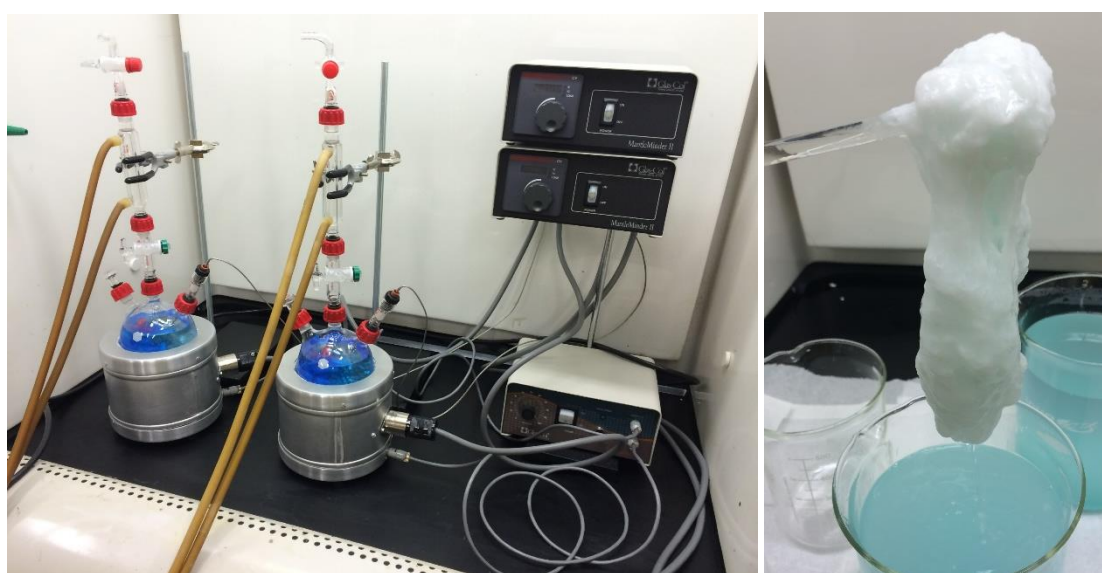


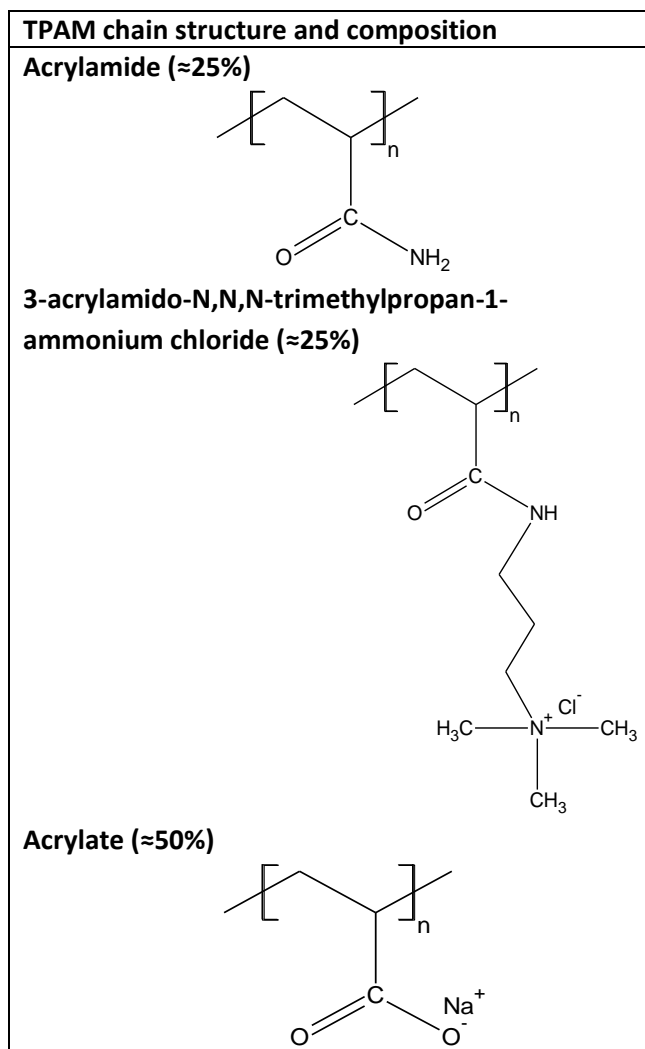
Figure 4.2. Synthesis of the terpolymer TPAM through hydrolysis with NaOH.

4.2. Experimental validation techniques

The structure and composition of the terpolymer TPAM synthesized was corroborated with two experimental techniques: nuclear magnetic resonance (NMR) and neutron activation analysis (NAA). From the synthesis procedure, the terpolymer structure and composition to be validated is summarized in **Table 4.1**. The validation

procedures aim at the detection of two key aspects: the presence of three distinct modules in the chain, and the percentage yield of the acrylate module.

Table 4.1. TPAM chain structure and composition.



4.2.1. Nuclear magnetic resonance (NMR)

NMR Spectra for nuclei of proton (^1H) and carbon isotope (^{13}C) were selected as the parameters for the validation of the molecule synthesized. The purpose of this methodology is to trace the different atomic groups that are required to be present in the

molecular structure through characterization of the peaks emitted by both (^1H and ^{13}C) isotopes. **Figure 4.3 (a)** illustrates the ^1H NMR spectrum for the terpolymer TPAM as well as **(b)** the ^{13}C spectrum. Although both spectra provide correct evidence of the desired structure, the key characteristic that ultimately validates the structure of the sample synthesized as a terpolymer is the presence of three peaks in the ^{13}C NMR spectrum between 175-185 ppm which corresponds to the carbonyl ($\text{C}=\text{O}$) region. This is because the detection of three distinct peaks corroborates that there were carbonyl groups pertaining to three different environments (or substructures) of different composition. If the synthesized product had been for example, a homopolymer such as polyacrylamide, only one carbonyl peak would have been detected. **Figure 4.3 (c)** illustrates in detail the carbonyl area with the three ($\text{C}=\text{O}$) peaks indicated with red arrows.

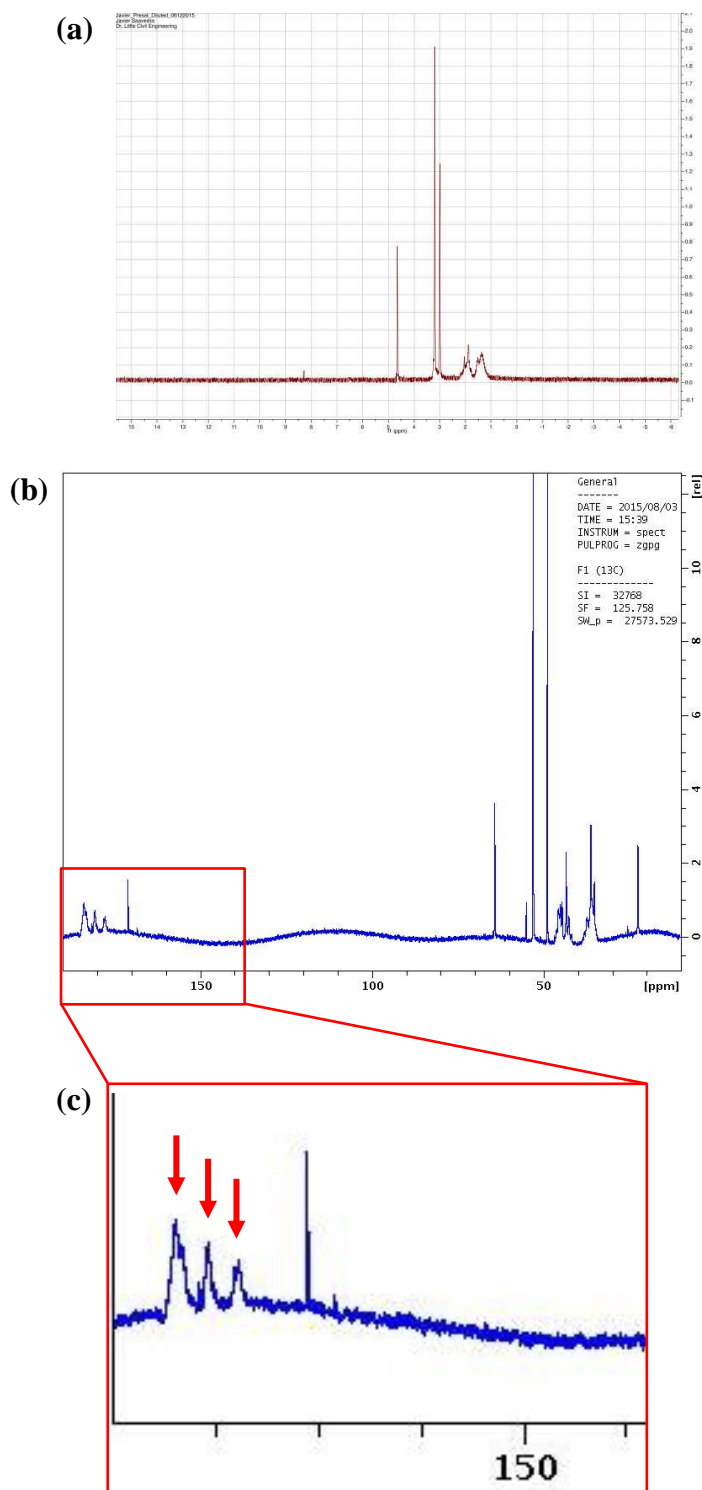


Figure 4.3. NMR spectra validating the structure and composition of the synthesized terpolymer TPAM. (a) ^1H spectrum, (b) ^{13}C spectrum, (c) three-peak carbonyl area detail.

4.2.2. Neutron activation analysis (NAA)

Within the different elemental analysis techniques, NAA is a multi-element analytical method that allows accurate determination of the concentration of a given element in a material. The method relies on a spectra of gamma radiation emitted by nuclei of any element when subjected to a beam of neutrons in a nuclear reactor ³⁰. The method has a wide range of applications including full elemental analyses of soils ³¹. One of the great advantages of the NAA method is the non-destructive nature of the procedure.

In the case of the terpolymer (TPAM), the NAA method was conducted to assess the amount of sodium (Na) that the anionic module is expected to yield as a verification of the final step of hydrolysis in the synthesis process. The NAA results yield therefore, the actual weight percentage of sodium (Na) per molar weight of the terpolymer molecule. In this particular study, a TPAM sample consisting of 1.0 g was prepared, for which the NAA results are shown in **Table 4.2**. Sodium content ranged between 7.29 - 7.44% (w/w) per TPAM repeating unit based on three measurements obtained from the same sample. This result is catalogued as consistent suggesting homogeneity for sodium (Na) for samples larger than 250 mg.

Table 4.2. NAA results showing the sodium content in the TPAM samples analyzed.

Sample #	Sample ID	%Na (w/w) ± SD
1	TPAM End Piece	7.44 ± 0.06
2	TPAM End Piece	7.29 ± 0.06
3	TPAM Middle Piece	7.40 ± 0.06

4.3. Insights from atomistic modeling

As the terpolymer TPAM represented a new formulation it was considered beneficial to explore its structure-composition behavior with molecular modeling techniques. Due to the macromolecular nature of the terpolymer the approach taken was classical mechanics modeling, and even with such approach it was only feasible to represent the terpolymer chains with pruned models. The repeating unit was investigated performing a geometry optimization with the COMPASSII force field to assess the intramolecular interactions between the three modules. These will tend to interact with one another in a self-solvation scenario (**Figure 4.4**).

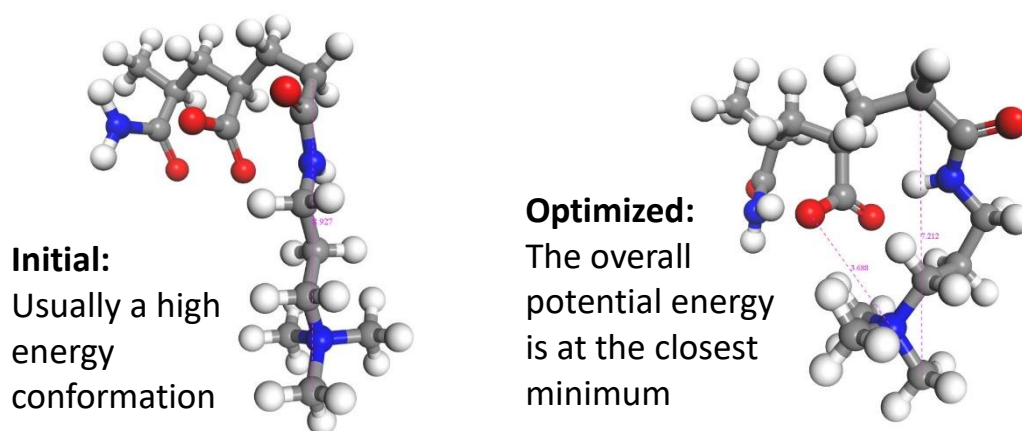


Figure 4.4. Intramolecular interactions between the three different modules in a TPAM repeating unit.

4.3.1. TPAM interactions with sodium montmorillonite

One of the aspects of interest in the study of the terpolymer was the characterization of the interaction of the TPAM polymer chains with soil minerals such as sodium montmorillonite that are problematic due to their creation of volumetric instability in soil structures. Two major questions were to be solved. First, is the TPAM

able to provide a hydrophobic shield to prevent water from swelling the montmorillonite interlayered structure? Second, is the TPAM able to interact with interlayer cations such as sodium (Na) and reduce the degree of hydration of the interlayer? To assess these interrogatives, molecular dynamics simulations (MD) of an aqueous TPAM-montmorillonite interface model were conducted. The model system comprised five molecular fragments of the TPAM repeating unit in solvation with interfacial water at the montmorillonite surface. Three different hydration conditions were simulated by increasing the amount of interfacial water molecules from 50, 100, to 250 molecules. The force field used was the INTERFACE force field. The thermodynamic ensemble adopted for the simulations was the NPT ensemble, allowing all cell dimensions to change, and the simulations were allowed to equilibrate over a period of 100 picoseconds (ps). **Figure 4.5(a through f)** illustrates the snapshots of the results of the MD simulation for the three water saturation conditions investigated. In a qualitative way, these results indicate that the TPAM chains are able to interact and sorb sodium (Na) cations present in the montmorillonite interlayer. However, it is unclear whether there is a definitive hydrophobic shielding effect because TPAM moieties also sorb water molecules at the interface.

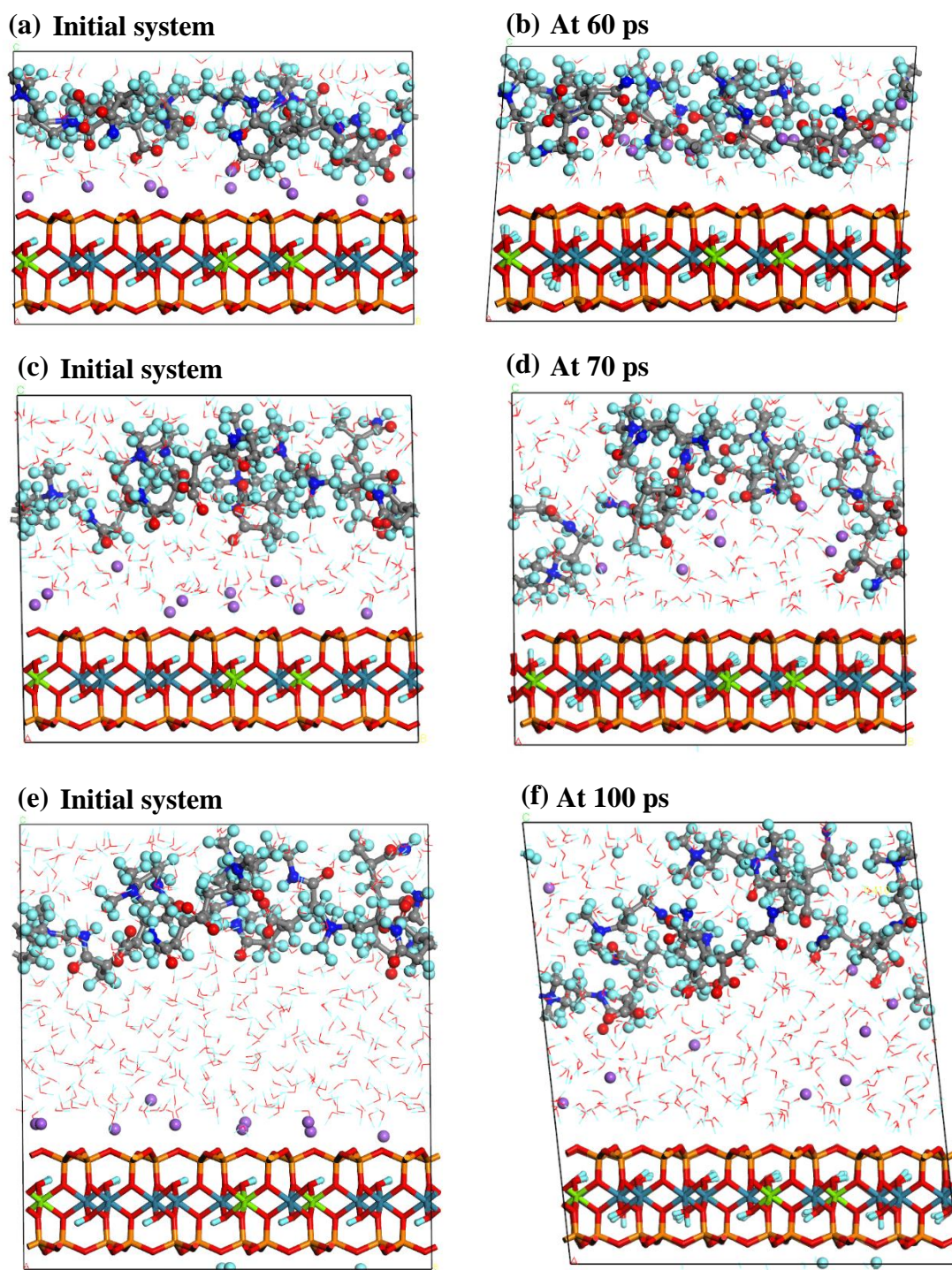


Figure 4.5. MD simulation snapshots: (a) and (b) for 50 waters, (c) and (d) for 100 waters, (e) and (f) for 250 waters. Atom colors are red (O), cyan (H), yellow (Si), grey (C), blue (N), purple (Na), green (Mg), and teal (Al).

5. CONCLUSIONS

Atomistic modeling methodologies are applicable to the study of chemical and physical interactions between infrastructure material constituents of both nature: mineral and organic. Furthermore, atomistic modeling techniques and methodologies enable mechanistic understanding of phenomena observed that would otherwise not be achieved with experimental methods or other modeling methodologies. This approach was successfully applied to asphalt/mineral filler and terpolymer/mineral systems.

5.1. Asphalt and mineral filler systems

- Classical mechanics simulations provide a sound understanding of surface interaction energies that only have non-bonding energy components such as Coulombic and van der Waals energies that properly define non-reactive systems. Therefore, parameters dependent upon surface area such as the work of adhesion and cohesion can be predicted effectively and efficiently.
- Although classical mechanics simulations allow more realistic representations of the crystallinity of mineral phases as well as the macromolecular structure of the asphalt organic phases, the impediment posed by the inability to model reactions causes limitations to properly evaluate reactive minerals such as hydrated lime and calcite.

- A major limitation of classical mechanics modeling is the dependence of the modeling approach on the existence of a force field expression tailored to the elemental composition of the atomistic system in study. If an adequate force field expression does not exist, then the process of developing one could be extremely time intensive.
- Despite the limitations found with classical mechanics modeling, the analysis methodology ranked the mechanisms of adhesion. Such ranking was, in order of decreasing work of adhesion: calcite > hydrated lime > quartz. The result that calcite has better adhesion than lime is explained by the difference in the surface composition of these minerals. The calcite surface has highly polar carbonate groups and calcium atoms exposed, whereas the surface of hydrated lime is composed hydroxyl groups with the hydrogen atoms facing outward, which makes a surface that can only interact through hydrogen bonding.
- Quantum mechanics modeling proved to be extremely useful as it enabled the adequate evaluation of the reactive behavior of mineral fillers such as hydrated lime and calcite and make a remarkable comparison with non-reactive minerals such as quartz.
- An advantage of the quantum modeling approach is the ability to surround the model molecular units with solvent continuums of different composition. In the case of this study, two solvents were investigated: water, and n-dodecane. The

first case (water) was used to represent a benchmark condition in which water has substantially infiltrated the asphalt matrix, whereas the second case in which n-dodecane was used represents the pure conditions in which asphalt exists. That is, a dispersion of larger macromolecules in a matrix of paraffinic molecules.

- The most important trend observed with quantum mechanics modeling in the case of the asphalt and hydrated lime interaction is the corroboration of preferential complexation with carboxylic acids, which corroborates the experimental data obtained by Petersen ⁷. Furthermore, the difference found between the dissociation energies of hydrated lime and the quartz model is substantial (of about nine-fold).
- An advantage found with quantum mechanics modeling, which is still under study, is the ability to evaluate the impact of the pH of the surrounding solvent. In the case of asphalt: $6 < \text{pH} < 9$. It was found that dissociation energy values change (increase) substantially when a mildly acidic condition is assumed. Simulations to evaluate mildly alkaline conditions are still under investigation.
- As a consequence of the ability to evaluate the pH of the solvent with quantum mechanics modeling, the calcite system was modeled and compared with the reactivity of hydrated lime against that of calcite. This elucidates the question: is it any better to use hydrated lime instead of calcite? The answer is yes, since

hydrated lime shows a dissociation energy approximately twice as large as that of calcite.

- The major limitation found with quantum mechanics modeling was the complexity generated for the usage of the approach to evaluate periodic systems. Therefore, simplified non-periodic molecular systems had to be formulated. While such simplification likely represents a radical deviation from the natural behavior of crystalline and amorphous periodic solid surfaces, the bonding environments could be mimicked with discrete molecular units in complexation with one another, and this allowed to draw marked trends between the potential reactive behavior of minerals such as hydrated lime, and calcite.

5.2. Terpolymer (TPAM) interaction with soil minerals

- With the use of specialized air-sensitive chemistry equipment the synthesis of a novel terpolymer (TPAM) was successful. Experimental validation data from NMR and NAA indicates that a tri-block co-polymer was present in the samples analyzed. The major evidence from the NMR data is the presence of three distinct peaks in the carbonyl region (175-185 ppm), which corroborate the presence of three carbonyl groups that belong to different chemical subunits. The major evidence from the NAA data is the constant value of sodium (Na) present in the sample analyzed, which corroborates that the hydrolysis reaction occurred

and the percent yield of anionic module (carboxylate) in the repeating unit of the terpolymer was correct.

- Classical atomistic modeling techniques corroborated the behavior of the groups present in the repeating units of the TPAM chains, which tend to interact with one another in a self-solvation scenario after a geometry optimization in gas phase. However, when a solvent is added such as water, some of these subunits will also unfold and interact with the solvent.
- The interaction of TPAM repeating units with sodium montmorillonite was qualitatively assessed with the use of classical molecular dynamics (MD) simulations. The results under different water saturation conditions indicate that the TPAM chains are able to interact and sorb interlayer cations such as sodium (Na). However, conclusions regarding the hydrophobic shielding effect are still unclear as the results indicate that the TPAM chains will also sorb water within the polymeric matrix and in between the polymer and the mineral surface.

REFERENCES

1. C. J. Cramer, *Essentials of computational chemistry: theories and models*, John Wiley & Sons, 2 edn., 2004.
2. E. Lewars, *Computational chemistry, Introduction to the theory and applications of molecular and quantum mechanics*, Springer Netherlands, 2 edn., 2011.
3. D. Sholl and J. A. Steckel, *Density functional theory: a practical introduction*, John Wiley & Sons, 2009.
4. H. Sun, Z. Jin, C. Yang, R. L. Akkermans, S. H. Robertson, N. A. Spenley, S. Miller and S. M. Todd, *Journal of molecular modeling*, 2016, **22**, 47.
5. D. N. Little and J. C. Petersen, *Journal of Materials in Civil Engineering*, 2005, **17**, 207-218.
6. D. Lesueur, J. Petit and H.-J. Ritter, *Road materials and pavement design*, 2013, **14**, 1-16.
7. J. C. Petersen, H. Plancher and P. M. Harnsberger, *Lime Treatment of Asphalt: Final Report. Lime Treatment of Asphalt to Reduce Age Hardening and Improve Flow Properties. Lime Treatment of Asphalt-aggregate Mixtures to Reduce Moisture Damage*, Western Research Institute, Laramie, Wyoming, 1987.
8. D. N. Little, D. H. Allen and A. Bhasin, *Modeling and design of flexible pavements and materials*, Springer, 2018.
9. R. T. Downs and M. Hall-Wallace, *American Mineralogist*, 2003, **88**, 247-250.
10. D. D. Li and M. L. Greenfield, *Fuel*, 2014, **115**, 347-356.
11. L. Zhang and M. L. Greenfield, *Energy & fuels*, 2007, **21**, 1712-1716.
12. H. Heinz, T.-J. Lin, R. Kishore Mishra and F. S. Emami, *Langmuir*, 2013, **29**, 1754-1765.
13. D. N. Little and A. Bhasin, *Using surface energy measurements to select materials for asphalt pavement*, Report NCHRP RRD 316, National Academy of Sciences, 2007.
14. G. Xu and H. Wang, *Computational Materials Science*, 2016, **112**, 161-169.

15. A. E. Alvarez, E. Ovalles and S. Caro, *Construction and Building Materials*, 2012, **28**, 599-606.
16. Y. Tan and M. Guo, *Construction and Building Materials*, 2013, **47**, 254-260.
17. R. E. Robertson, J. Branthaver, H. Plancher, J. Duvall, E. Ensley, P. Harnsberger and J. Petersen, *Chemical properties of asphalts and their relationship to pavement performance*, Report SHRP-A/UWP-91-510, Strategic Highway Research Program, National Research Council Washington, DC, 1991.
18. S. Alam and Z. Hossain, *Construction and building materials*, 2017, **152**, 386-393.
19. J. P. Perdew, K. Burke and M. Ernzerhof, *Physical review letters*, 1996, **77**, 3865.
20. J. P. Perdew, K. Burke and M. Ernzerhof, *Errata:(1997) Phys Rev Lett*, 1996, **78**, 1396.
21. A. Becke, *Chem. Phys*, 1993, **98**, 5648.
22. A. D. Becke, *Physical review A*, 1988, **38**, 3098.
23. C. Lee, W. Yang and R. G. Parr, *Physical review B*, 1988, **37**, 785.
24. R. Ditchfield, W. J. Hehre and J. A. Pople, *The Journal of Chemical Physics*, 1971, **54**, 724-728.
25. A. V. Marenich, C. J. Cramer and D. G. Truhlar, *The Journal of Physical Chemistry B*, 2009, **113**, 6378-6396.
26. S. Fliszár, *Atomic charges, bond properties, and molecular energies*, John Wiley & Sons, 2009.
27. J. B. Foresman and A. Frisch, *Exploring chemistry with electronic structure methods*, Gaussian, Inc., Wallingford, CT USA, 3 edn., 2015.
28. M. J. Frisch, G. W. Trucks, H. B. Schlegel, G. E. Scuseria, M. A. Robb, J. R. Cheeseman, G. Scalmani, V. Barone, G. A. Petersson, H. Nakatsuji, X. Li, M. Caricato, A. V. Marenich, J. Bloino, B. G. Janesko, R. Gomperts, B. Mennucci, H. P. Hratchian, J. V. Ortiz, A. F. Izmaylov, J. L. Sonnenberg, Williams, F. Ding, F. Lipparini, F. Egidi, J. Goings, B. Peng, A. Petrone, T. Henderson, D. Ranasinghe, V. G. Zakrzewski, J. Gao, N. Rega, G. Zheng, W. Liang, M. Hada, M. Ehara, K. Toyota, R. Fukuda, J. Hasegawa, M. Ishida, T. Nakajima, Y. Honda, O. Kitao, H. Nakai, T. Vreven, K. Throssell, J. A. Montgomery Jr., J. E.

- Peralta, F. Ogliaro, M. J. Bearpark, J. J. Heyd, E. N. Brothers, K. N. Kudin, V. N. Staroverov, T. A. Keith, R. Kobayashi, J. Normand, K. Raghavachari, A. P. Rendell, J. C. Burant, S. S. Iyengar, J. Tomasi, M. Cossi, J. M. Millam, M. Klene, C. Adamo, R. Cammi, J. W. Ochterski, R. L. Martin, K. Morokuma, O. Farkas, J. B. Foresman and D. J. Fox, *Gaussian 16 Rev. C.01*, Wallingford, CT, 2016.
29. M. L. Patrizi, M. Diociaiuti, D. Capitani and G. Masci, *Polymer*, 2009, **50**, 467-474.
30. M. D. Glascock, in *Encyclopedia of Global Archaeology*, ed. C. Smith, Springer New York, New York, NY, 2014, DOI: 10.1007/978-1-4419-0465-2_337, pp. 5239-5247.
31. A. El-Taher and M. A. K. Abdelhalim, *Journal of Radioanalytical and nuclear chemistry*, 2014, **300**, 431-435.